Broadband Optical Supercontinuum Generation Using Low-Cost Multimode 975-nm Pump Lasers

Zhejing Jiao

A Thesis

In the Department

of

Electrical and Computer Engineering

Presented in Partial Fulfillment of the Requirements

For the Degree of Master of Applied Science at

Concordia University

Montréal, Québec, Canada

November 2008

Your file Votre référence
ISBN: 978-0-494-63225-3
Our file Notre référence
ISBN: 978-0-494-63225-3

ABSTRACT

Broadband Optical Supercontinuum Generation Using

Low-Cost Multimode 975-nm Pump Lasers

Zhejing Jiao

Broadband laser sources are very attractive for optical communications and technologies requiring low-coherence laser sources. The supercontinuum (SC) is generated by ultra-short pulsed or continuous wave (CW) lasers that are injected into fibers with high nonlinearity. Mode-locked lasers and Raman fiber lasers are generally used in the two pumping regimes. Pumping with 975-nm multimode laser diode is considered a low cost technology in the CW regime. However, it has not been well investigated.

This thesis studies the SC generation process using low-cost 975-nm multimode laser diodes, a piece of Erbium/Ytterbium co-doped fiber (EYDF) and two units of highly nonlinear fibers (HNLFs) with different dispersion properties around 1550nm wavelengths.

Three broadband and high optical power SCs extending to 2000nm wavelength are successfully generated, one in ring and two in single-line structure. To our knowledge, they are the broadest SCs using this low cost technology. In addition, one of the two SCs in the single-line structure even covers a wavelength range from 1200nm to more than 2000nm by getting rid of the band limit of splitter. Moreover, the key role of four-wave mixing (FWM) in the broadness and flatness of CW pumped SC are demonstrated. The demonstration is more evident than previous works and convergence is obtained in the two pumping regimes on the importance of FWM in SC generation.

Our designs realize fiber laser sources with high power, broad bandwidth and reduced cost.

Acknowledgements

I would like to express my sincere gratitude to my supervisor Dr. X. Zhang for his guidance, advice and financial support for me to finish this thesis.

I thank P. Long, President of O/E land Inc., for his support and help in my experiment and also J. Carignan, for his technical suggestions on the practical operations.

I have sincere appreciation to the Canadian Institute for Photonic Innovations and O/E Land Inc., Montreal for supporting this research project.

Last but not least, I am very grateful to my mother for her love and support throughout my life.

Table of Contents

List of Figures

List of Tables

List of Acronyms

ASE	Amplified Spontaneous Emission
CW	Continuous Wave
DC	Direct Current
DCF	Double-Cladding Fiber (in the combiner)
DCF	Dispersion Compensating Fiber
DSF	Dispersion-Shifted Fiber
EDF	Erbium Doped Fiber
EYDF	Erbium/Ytterbium Co-doped Fiber
FWM	Four-Wave Mixing
GVD	Group Velocity Dispersion
HNL-DFF	Highly-Nonlinear Dispersion-Flattened Fiber
HNLF	Highly Nonlinear Fiber
MI	Modulation Instability
NA	Numerical Aperture
OCT	Optical Coherence Tomography
OSA	Optical Spectrum Analyzer
PCB	Printed Circuit Board
PCF	Photonic Crystal Fiber
RFL	Raman Fiber Laser
SBS	Stimulated Brillouin Scattering
SC	Supercontinuum
SLED	Superluminescent Diode
SMF	Single Mode Fiber

SPM	Self-Phase Modulation
SRS	Stimulated Raman Scattering
WDM	Wavelength Division Multiplexing
XPM	Cross-Phase Modulation

List of Principal Symbols

A	Ampere
A_{eff}	Effective Area (μm^2)
D	Dispersion Parameter ($ps/(nm \cdot km)$)
D_M	Material Dispersion ($ps/(nm \cdot km)$)
D_W	Waveguide Dispersion ($ps/(nm \cdot km)$)
Er	Erbium
g_R	Raman-gain Coefficient (m/W)
g_R / A_{eff}	Normalized Raman-gain Coefficient $(W \cdot km)^{-1}$
g_B	Brillouin-gain Coefficient (m/W)
$\hbar$	The Reduced Planck Constant ($6.582 \times 10^{-16} eV \cdot s$)
$\hbar\omega$	Photon Energy
K_1	Cross Relaxation Coefficient, Energy Transfer from Er^{3+} to Yb^{3+}
K_{-1}	Cross Relaxation Coefficient, Energy Transfer from Yb^{3+} to Er^{3+}
K_2	Cross Relaxation Coefficient, Secondary Energy Transfer from Yb^{3+} to Er^{3+}
Δk_M	Phase-matching Contribution from Material Dispersion (cm^{-1})
Δk_{NL}	Phase-matching Contribution from Waveguide Dispersion (cm^{-1})
Δk_W	Phase-matching Contribution from Nonlinear Effects (cm^{-1})
L_{eff}	Effective Interaction Length (km)
s	Dispersion Slope ($ps/(nm^2 \cdot km)$)
$\overline{n_2}$	Nonlinear-index Coefficient (m^2/W)

Yb	Ytterbium
λ	Wavelength (nm)
ω	Frequency (TH_z)
β	Propagation Constant (radians/meter)
α	Fiber loss (dB/km)
β_2	GVD Coefficient (ps^2/km)
$\lambda_{ZD}(\lambda_0)$	Zero Dispersion Wavelength (nm)
γ	Nonlinear Coefficient $(W \cdot km)^{-1}$
Ω	Frequency Difference between two Lights

CHAPTER 1 INTRODUCTION

1.1 Background and Applications

Supercontinuum (SC) laser is a laser source with very broad spectral width. Its bandwidth could reach as large as 1000nm, which is very remarkable compared to other regular broadband sources like incandescent lamps, amplified spontaneous emission (ASE) light and superluminescent diodes (SLED) as shown in Fig. 1.1. The C band and L band ASE covers from 1530nm to 1625nm and is usually generated from Erbium doped fiber amplifier (EDFA). SLED is a laser diode without optical feedback and its optical bandwidth is of tens of nanometers. Incandescent lamp is what we use in the normal life. Its beam is not focused, the power is very low and the light could not be used in the communication field.

Besides the broad bandwidth, SC has other characteristics, such as low temporal coherence, high spatial coherence, high output power and flexible spectral coverage. These make it very desirable and attractive in many applications. For example, in optical coherence tomography (OCT), higher resolution and scan rate are achieved by using SC source. The axial resolution of a typical OCT system is about 10μm with 1kHz axial-line scan rate. These two parameters are improved to be better than 2μm and more than 10kHz respectively with broadband SC [41]. In the field of telecommunications, ultra broadband wavelength-division-multiplexed (WDM) systems are based on SC to create a series of WDM channels [2-3]. The SC spectrum can be sliced into many frequency channels by a series of filters. The wide bandwidth of SC increases the number of channels and realizes high system capacity in low costs and reliability [2]. Also, laser

sources with wavelengths of longer than 1750nm are required to "write" gratings operating in that optical band. Moreover, SC source is used in optical sensing, imaging system [4] and metrology [5], etc.

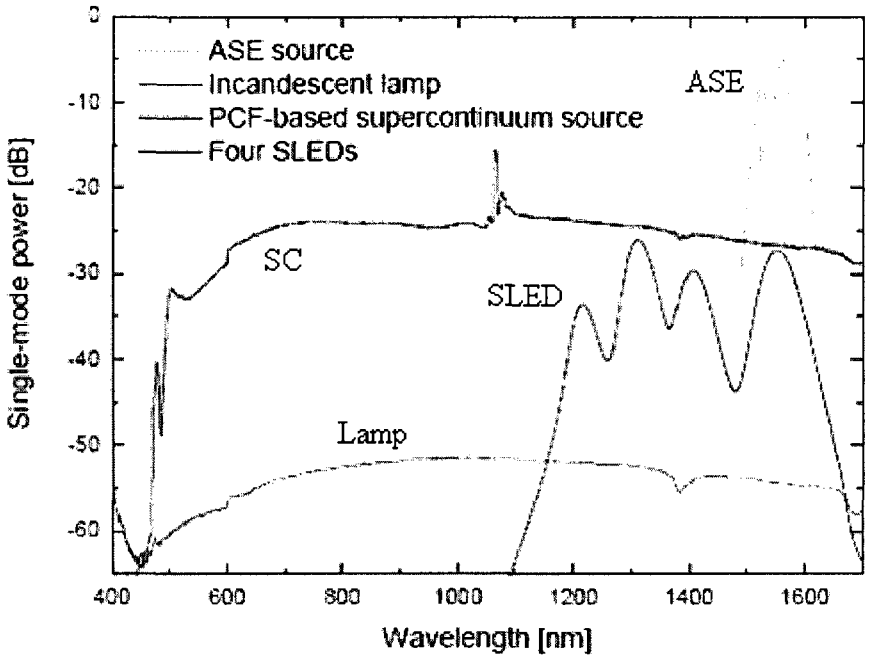

Figure 1.1: Comparison of four broadband sources in the frequency domain [1].

1.2 Review Technologies and Motivation

Since the first SC generation was demonstrated by Alfano and Shapiro [6] in the early 1970s, it has been always an attractive topic in the optical field. The continuum is generated by pumping a laser beam into a specialty fiber and many nonlinear effects are involved in the broadening process, such as self-phase modulation (SPM), cross-phase modulation (XPM), stimulated Raman scattering (SRS), modulation instability (MI), four-wave mixing (FWM), etc. The specialty fibers usually used are photonic crystal fiber (PCF) and highly nonlinear fiber (HNLF) with high nonlinearities and low

dispersion parameters around the desired pumping wavelength. Generally, three types of laser sources are taken as pumps that are injected to the specialty fiber to generate SC:

- Nanosecond to tens of femtosecond mode-locked lasers [7-11]
- Raman fiber lasers [12-16]
- 975-nm multimode laser diodes [17]

The first two laser sources have been widely used in the pulsed and continuous wave (CW) pumping regimes respectively. Mode-locked lasers could deliver high peak power from hundreds of watts to kilowatts and generate very wide SC spectrum. But the generated SC has complex spectral structure [4] and the average spectral density is relatively low from -20 to -10dBm/nm [7, 31]. Raman fiber laser has high relative intensity noise level and could deliver several-Watt average powers at many wavelengths to generate Watt-level SC efficiently. These two pump sources have been widely used in previous works with different structures by taking HNLF or PCF as the nonlinear medium. Some of the generated SC has reached wavelength of 2000nm but setups are generally very expensive.

On the other hand, pumping with 975-nm multimode lasers is considered low-cost technology and has not been investigated intensively. The first SC pumped by 975nm multimode pump laser diodes was proposed by J. Lee in 2006 [17]. With the ring structure, a broadband SC from 1300nm to 1750nm was generated, which demonstrated the practicality of SC generation in low-cost devices. But the optical output power of SC was very low, only about 53.4mW. Further study on this low cost technology with the ring structure extended spectrum to wavelength of ~1850nm and increased output power to 72.6mW in 2007 [40]. However, compared to SCs pumped by the mode-locked lasers

and RFLs, the spectrum still has not reach wavelength of 2000nm yet and power is only of tens of milliwatt. Fiber loss increases very fast from wavelength of 1750nm to 2000nm and SC spectrum is relatively difficulty to be extended to that wavelength region. Thus more research has to be done to develop potential of this low cost pumping scheme.

1.3 Thesis Scope and Contributions

The focus of this research work is on designing simple and economical broadband laser sources for many applications. Instead of using high power and efficient but expensive ultra-short pulses and CW Raman fiber lasers, we consider the use of 975-nm multimode laser diodes, a piece of Erbium/Ytterbium co-doped fiber (EYDF) amplifier and HNLF to generate low cost, high power and broadband continuum spanning over 1000nm. The major challenge in this case is how to assemble the three main components together with other passive components and get optimum results on both spectrum and optical power. Three design schemes are investigated and roles of nonlinear effects in the broadening process are compared and analyzed. The conclusion regarding their effects on SC generation pumped by CW is thought to be useful in guiding future researches.

The main contributions of this thesis are:

1. Analysis and design of a low cost, Watt-level and ~700nm wide CW pumped fiber ring laser experimentally. To our knowledge, it is the first SC extending to 2000nm in wavelength pumped by 975-nm multimode laser diodes.
2. Demonstrate the key role of FWM effect in the CW pumped SC broadening by employing two HNLFs with different dispersion parameters around wavelength of 1550nm. It is more evident than the former works [12] and coincides with the

demonstration of the importance of FWM in ultra-short pulse based SC generation [18].

3. Broadband SC is also generated with the same main components using single-line structure. Especially, the backward ASE driven SC gets rid of the band limit from splitters in the ring structure and covers a wavelength range from 1200nm to more than 2000nm.

1.4 Thesis Outline

The rest of the thesis is organized as follows.

Chapter 2 shows our three design structures and explains function of each component in the setup combined with relevant physical mechanisms for broadening. Theoretical basis on the component combinations and practical compatibility are also discussed.

Chapter 3 presents our experimental results using the ring structure. Different splitting ratios are used to divide optical light into two parts and the generated SCs are compared. The effect of splitting ratios on the SC generation in the ring structure is obtained and the optimum splitting ratio is also found. With the fixed optimum ratio, two HNLFs and their combinations are used in the ring to investigate different roles of nonlinear effects on the SC generation with CW pumps, i.e. SPM, XPM, SRS, MI and FWM. It is demonstrated that FWM plays a critical role in the flatness and broadness of the optical spectrum.

Chapter 4 presents generated SCs in the single-line structure. Two designs are used in this structure. It proves our conclusion on the importance of FWM effect again.

And an even broader SC of over 800nm wide in wavelength is observed on the optical spectrum analyzer (OSA).

Chapter 5 summarizes the results obtained and future work is also suggested.

CHAPTER 2 EXPERIMENTAL SETUPS AND BACKGROUND THEORIES

In this chapter, three different design schemes are investigated to generate SC. The first design is based on the ring structure as depicted in Figure 2.1. The SC generator consists of 15-m EYDF, two multimode 975-nm pump lasers, an optical fiber pump combiner, HNLF, an optical power splitter and an optical isolator. Two units of HNLFs with different dispersion characteristics are used as the nonlinear media to generate SC. The light from HNLF is split into two parts via the fiber splitter. One part is taken as output and the other is fed back to form the ring cavity. Different splitting ratios are used. And with the same main components, the other two designs based on the single-line structure are shown in Figure 2.2(a) and (b). In Fig. 2.2(a), HNLF is removed from the ring cavity and pumped by the EYDF ring laser while in Fig. 2.2(b) the continuum is directly driven by ASE from EYDF. It is known that in Erbium doped fibers (EDF), forward pumping has lower noise figure while backward pumping provides higher saturated output power [38]. EYDF is similar to EDF and therefore we considered backward pumping in our ASE driven SC to generate higher gain.

Table 2.1 lists all equipments used in our experiment. The main components for both structures are the same, including two multimode pumps at 975-nm, 15-m EYDF and two units of HNLFs. The generation principle in short is that 975-nm pump power is transferred to ~1550-nm ASE after propagating in EYDF, and then the ASE is broadened by various nonlinear effects in HNLF to generate SC. The function of each component as

well as physical mechanisms will be explained in detail in this chapter and then SC performance in the three designs will be analyzed in Chapter 3 and Chapter 4.

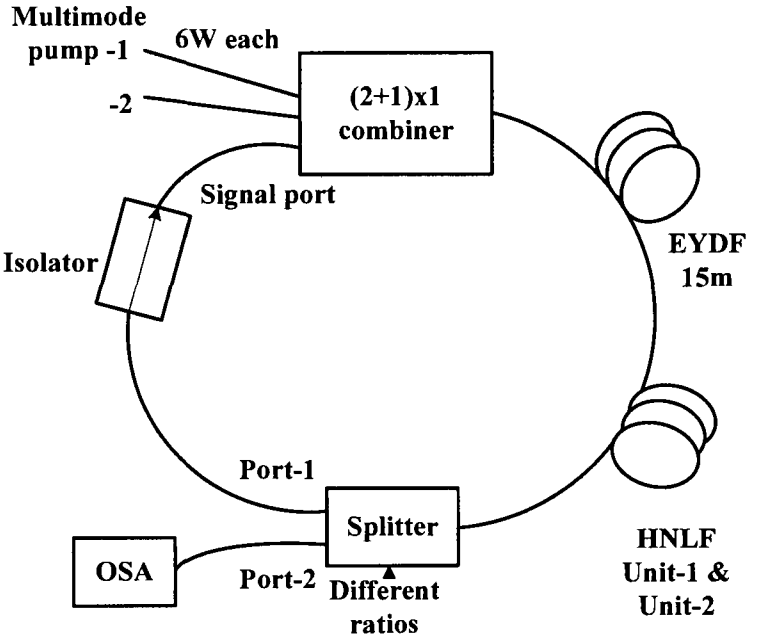

Figure 2.1: Experimental setup of the fiber ring laser.

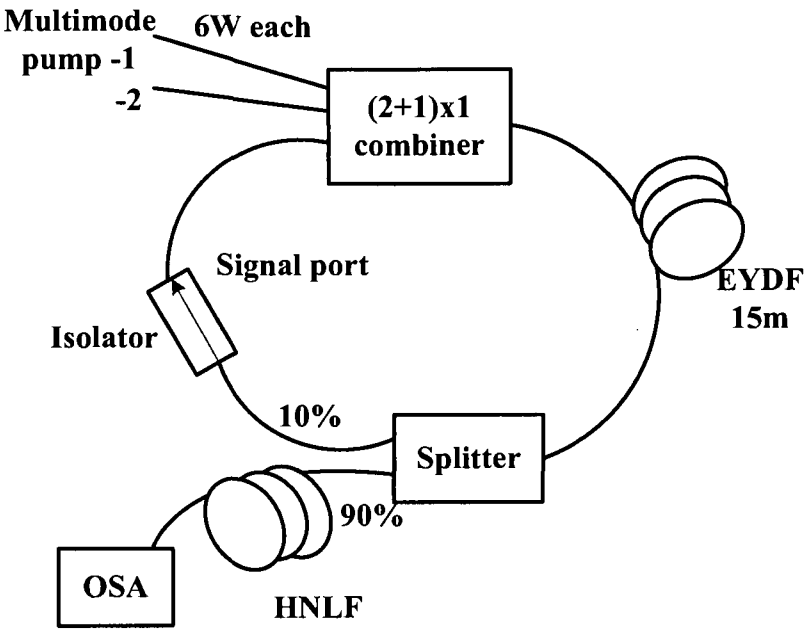

(a)

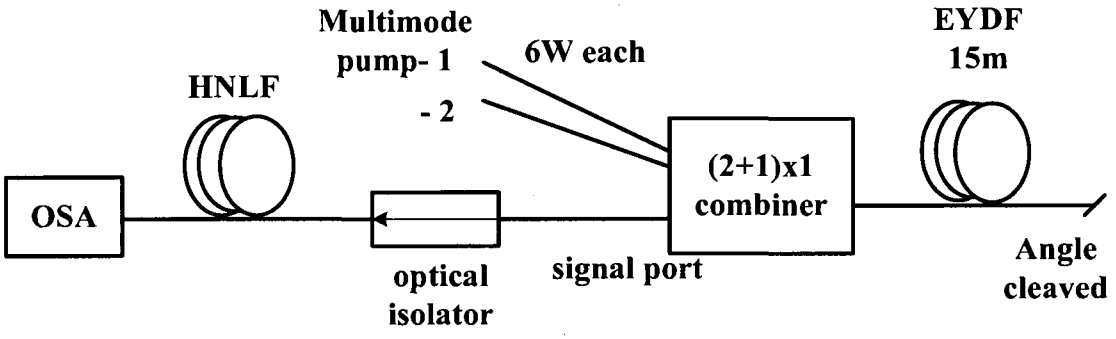

(b)

Figure 2.2: Experimental schematics of the single-line structure using (a) EYDF ring and (b) backward ASE.

Table 2.1: List of equipments used in our experiment.

Equipment	Producer	Function
DC power supply (maximum current 6A)	BK precision 1672	Provide 5V DC voltage for the laser driver
DC power supply (maximum current 5A)	ABRA AR-5ps-D	Provide current for fans
High Power Laser driver	O/E land Inc.	Provide stable current for 975nm pump laser
Multimode Pump laser at 975nm	EM4 EM304	Pumping source
(2+1)x1 Multimode Combiner	Avensys Tech.	Combine 975-nm pump and ~1550nm signal
Erbium/Ytterbium Codoped fiber	OFS EY125-SM-S	Amplifier C and L band light
Highly Nonlinear Optical Fibers	Sumitomo Electric Industries, Ltd.	Nonlinear media for spectral broadening
Optical Power Meter	Newport Model 1830-C	Detect laser power less than 200mW (640nm-1600nm)
Laser Power Meter (for high optical power)	Gentec PS-300WB	Detect high laser power (190nm-10μm)
Optical Spectrum Analyzer (OSA)	ANDO AQ-6315A	Observe SC spectrum (350nm-1750nm)
Optical Spectrum Analyzer (OSA)	Yokogawa AQ6375	Observe wider SC spectrum (1200nm-2000nm)

2.1 Multimode Pump

Two multimode laser diodes at 975 nm, each with maximum output power of 6W, are taken as pumps as shown in Fig. 2.3. The laser is placed on a heat sink. PGS (thermally conductive pyrolytic graphite sheet) between the module and the heat sink is used for the purpose of firm contacting. In addition, a fan is placed under the heat sink.

They are used to protect the laser from high temperature damage as well as to prevent the wavelength shift. The printed circuit board (PCB) in Fig. 2.3 is used as laser drive to provide stable current output for lasers. The drive current on the laser is varied by adjusting two potentiometers on the board and pump power is changed with the drive current. They are continuous wave pumps and the optical spectrum is given in Fig. 2.4. Optical and electrical parameters for the laser operation are listed in Appendix A. For 6W optical output, 8A current should be provided to each pump laser by the DC power supply. However, the current of the power supplies in our experiment could only go up to 6A, so the maximum output optical power is ~4.5W. Optical power is coupled into the combiner through a multimode fiber pigtail with 0.15 numerical aperture (NA). NA is the parameter to evaluate the percentage of a light source that could be coupled into the fiber.

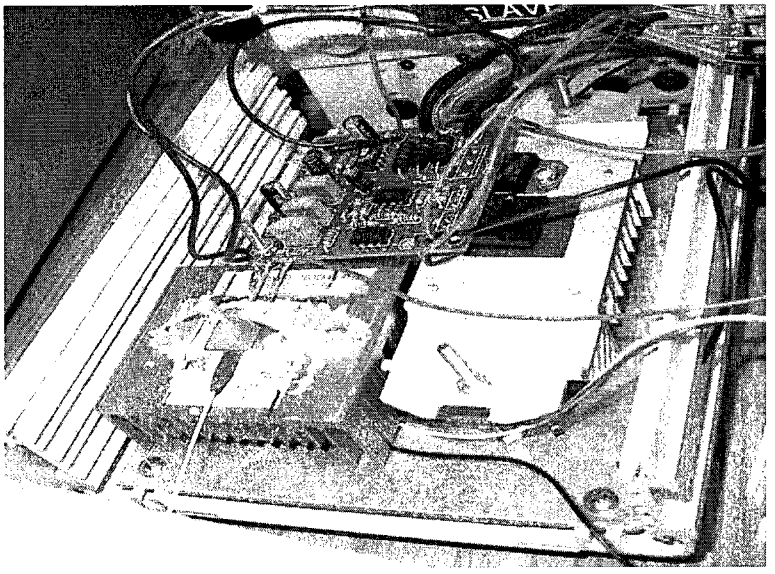

Figure 2.3: 2 pin multimode pump laser and the drive circuit that provides stable current.

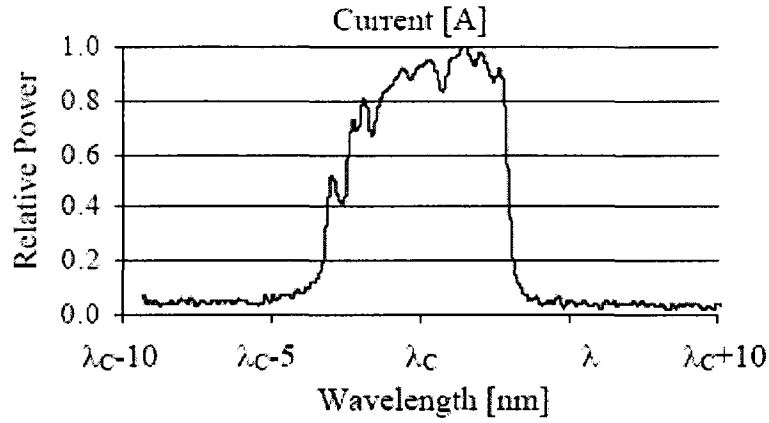

Figure 2.4: Optical spectrum of CW multimode pump lasers ($\lambda_c = 975nm$), from datasheet of EM4.

2.2 $(2+1)\times 1$ Multimode Combiner

As seen in Fig. 2.5, the combiner has three input ports, two for two multimode pumps around 900-1000nm and one for the signal input at 1530-1560nm. Core/cladding diameters of the two pump ports are 105/125μm and NA equal to 0.22, which are compatible with the pigtails of the two pump lasers. The large multimode core also facilitates high efficiency coupling. The maximum optical injection power of each pump port of the combiner is 7W, which is sufficient for a 6W injection. As seen from the datasheet in Appendix B, pumps and signal could propagate to the output port with low insertion loss and at the same time back reflection to the pump lasers is avoided by 40dB return loss. For the signal and output ports, two NAs are specified whereas the two pump ports have only one each. This is because the pigtails of the signal and output ports are double cladding fiber (DCF). DCF is single mode fiber but with low index coating outside. Refractive index of the outside coating is lower than the first cladding and light could propagate in both core and cladding. In the output port as well as in the EYDF, multimode pump light propagates in the first cladding and signal is confined in the core.

High multimode pump light then couples into the core gradually and is efficiently absorbed in the EYDF. This combiner is designed for the combination of the multimode pumps and the double-cladding EYDF fiber.

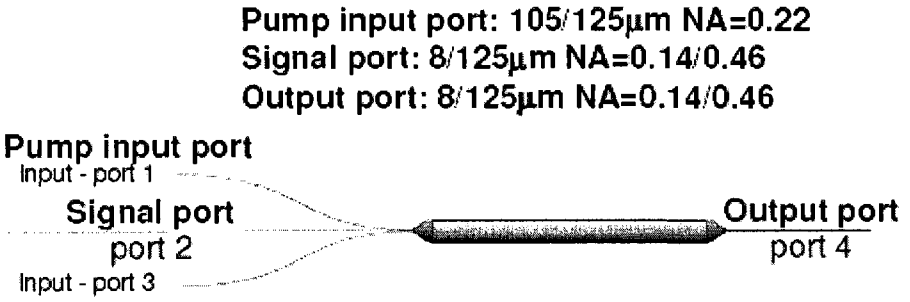

Figure 2.5: Illustration of the $(2+1)\times 1$ multimode combiner with three input ports and one output port. Three parameters of the fiber pigtail of each port are given, from datasheet of Avensys.

2.3 Erbium (Er)/Ytterbium (Yb) Co-doped Fiber (EYDF)

In the experiment, this co-doped fiber is used to absorb 975-nm pump and amplify light at ~1550nm.

2.3.1 Definition of EYDF

EYDF is a fiber by doping both Er and Yb ions into the fiber core area. The co-doping mechanism is based on the fact that the ${}^4I_{11/2}$ level of Er^{3+} and the ${}^2F_{5/2}$ level of Yb^{3+} are closely resonant in energy. Absorption efficiency of Er ions at 975nm is very low especially with the co-doping of Yb ions. So when pumped at around 975nm, Yb ions absorb most of the pump light and transfer part of the energy to Er^{3+}. Then Er ions emit amplified light at around 1550nm through stimulated or spontaneous emission.

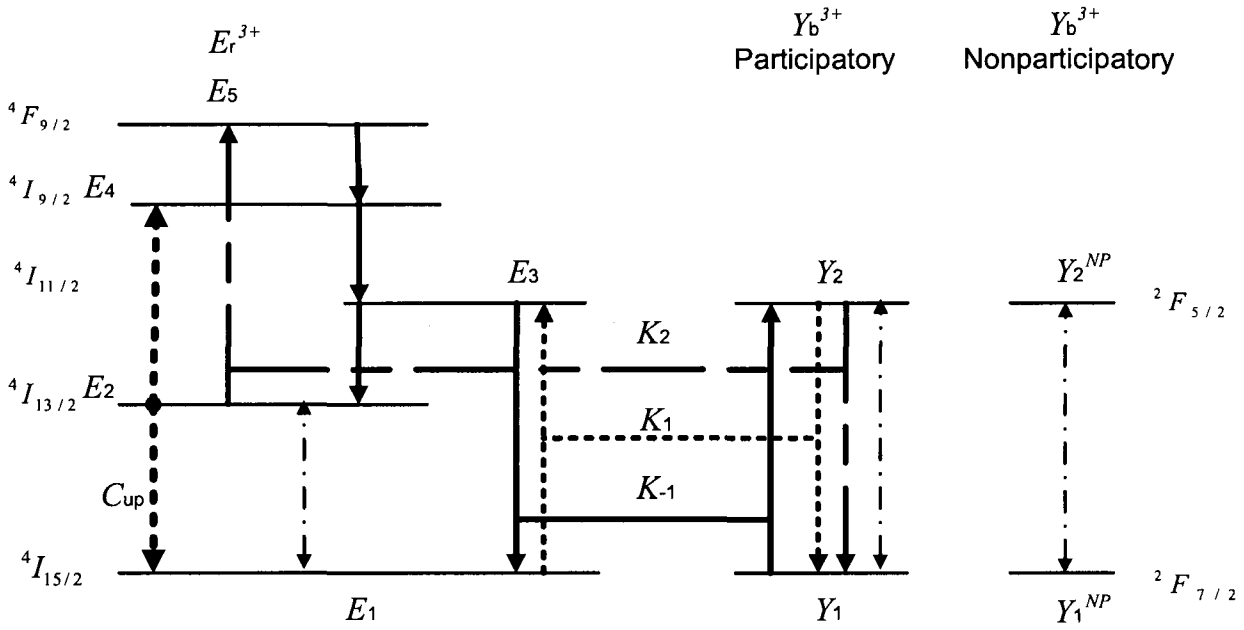

Figure 2.6: Energy level diagram of Er and Yb [19].

2.3.2 Energy Transfer Processes in EYDF [19, 20, 22]

Figure 2.6 shows energy levels in an Er-Yb system. There are three main cross-energy transfer progresses in this co-doped fiber. They are defined by cross relaxation coefficients K_1, K_{-1} and K_2, respectively.

For the process described by the coefficient K_1, Yb^{3+} at the ground state $^2F_{7/2}$ firstly absorbs pump light and is excited to the $^2F_{5/2}$ state. From there, the cooperation energy transfer between levels Y_2 and E_3 excites Er^{3+} from the ground level $^4I_{15/2}$ to the $^4I_{11/2}$ state while dropping back Yb^{3+} to the ground state of $^2F_{7/2}$.

The backward energy transfer is defined by the coefficient K_{-1}. Er^{3+} jumps from $^4I_{15/2}$ to the excited $^4I_{11/2}$ state by absorbing pump photons, and then relaxes to the

ground level by transferring energy to Yb^{3+} to be jumped to $^2F_{5/2}$. But with the doping of Yb, Er absorption at 975 nm is much reduced in the EYDF.

The coefficient K_2 describes the secondary energy transfer process from Yb ions at the excited $^2F_{5/2}$ level to Er ions at the $^4I_{13/2}$ state. Ytterbium ions relax to the ground state $^2F_{7/2}$, and Er ions are excited to the $^4F_{9/2}$ state. Then the Er^{3+} ions return back to the $^4I_{13/2}$ level nonradiatively, which wastes Yb^{3+} ions and decreases conversion efficiency.

Besides, other processes such as absorption, stimulated emission and spontaneous emission within the same ions of Yb^{3+} and Er^{3+} still occur.

Fig. 2.7 shows Er gain and absorption curves in EYDF as a function of wavelengths around 1550nm, based on which the performance of an EYDF is evaluated. Although transferring efficiency from Yb^{3+} to Er^{3+} ions is not 100%, peak absorption at 1530nm of Er ions can reach 35dB/m whereas for normal EDF, it is less than 10dB/m for C band amplifiers and around 20dB/m for L band amplifications.

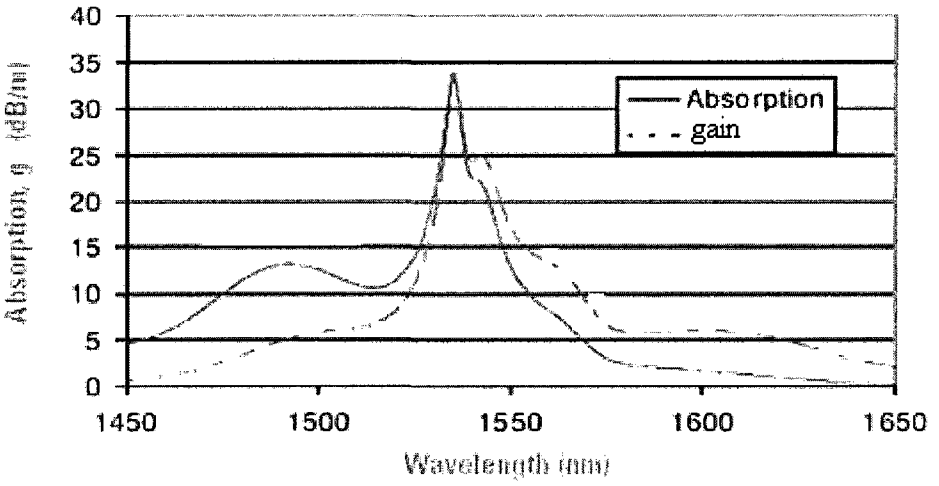

Figure 2.7: Gain and absorption coefficients of Er ions in the EYDF [24].

2.3.3 Advantages of Yb Sensitized EYDF

- **Wide Wavelength Selection in Pumps**

Compared to Er ions, Ytterbium has a wide absorption band from 800 to 1100nm, which provides flexibility in choosing suitable pump laser sources, such as Nd:YAG lasers at 1064nm, Nd-doped double-clad lasers, and high pump lasers at 975nm, etc[23].

- **Realizing Higher Er Doping than EDF**

Currently, Erbium doped fibers are normally used for pump powers of less than 1W. Higher Er ion doping could increase the gain. But when Er ions are highly doped to a silica core they form clusters, which cause concentration quenching. Distance between two adjacent ions decreases and two Er ions at the state $^4I_{13/2}$ will interact in a process called cooperative upconversion. In this process, one ion relaxes to the ground state by exciting the other one to the $^4I_{9/2}$ level. Then the excited ion at the $^4I_{9/2}$ state nonradiatively decays to the $^4I_{13/2}$ state. This greatly reduces conversion efficiency in the EDF. By adding Yb ions, Er ions are surrounded by the Yb ions and separated from each other. Quenching effects are strongly mitigated. And higher Er^{3+} concentration and gain are realized in the EYDF.

- **Higher Pump Power Absorption in Co-Doped Double-Cladding Fiber [21]**

The EYDF used in our experiment is a double cladding fiber. Multimode pumps are used instead of single mode pumps. In a single mode fiber, light only transmits in the small 8μm core. High power absorption is limited in such a single mode core. With multimode pumps and the double cladding, light propagates in the 125μm first-cladding and gradually coupled into the core to be efficiently absorbed. Figure 2.8 presents the cross-section of our Er/Yb co-doped fiber from OFS. Multimode pumps propagate in the

much larger shaded area that is the first-cladding. Increasing in the absorption efficiency can be roughly estimated by the square ratio of the two diameters that is $(\frac{125}{8})^2$. The star shape of the first cladding is also advantageous for high absorption. Er peak absorption at 1530nm is as high as 48dB/m. Special splicing program is required for splicing this double-cladding, star-shape and co-doped fiber. Controlling on prefuse time, prefuse current, gap, overlap, fusion time and fusion current is essential and very important for low loss splicing. More detailed data regarding to this co-doped fiber could also be found in Appendix C.

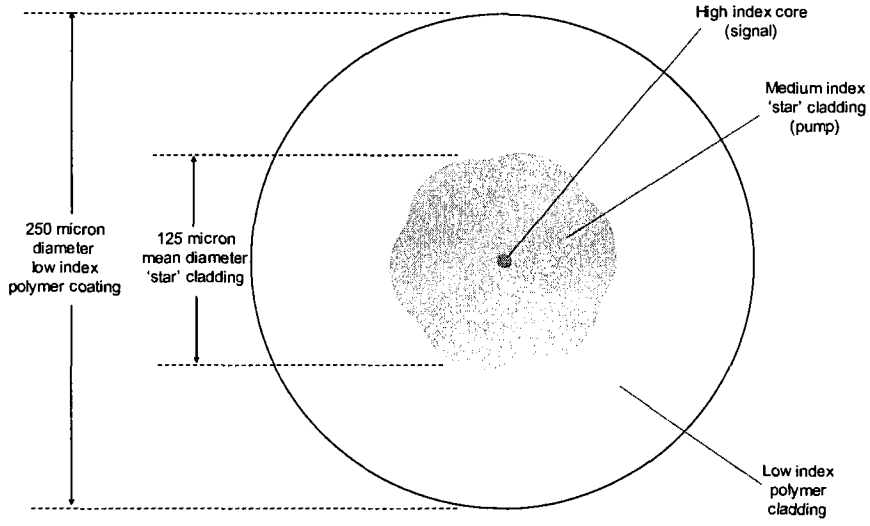

Figure 2.8: Cross-section of the star-shape double cladding Er/Yb codoped fiber from OFS datasheet.

2.4 Highly Nonlinear Optical Fiber (HNLF)

HNLF is an essential component in the SC generation. Many nonlinear effects occur in this specialty fiber and lead to spectral broadening.

2.4.1 Dispersion and Nonlinear Effects [25, 35, 36]

- **Group-Velocity Dispersion (GVD)**

When an optical wave is injected into the fiber, the response of the medium depends on the optical frequency ω. As a result, the refractive index of the fiber is a function of ω. This property is referred as chromatic dispersion. Due to chromatic dispersion, different spectral components of the light propagate at different group velocities and are given by $c/n(\omega)$. This phenomenon is called GVD. The total dispersion includes two parts, material dispersion and waveguide dispersion, $D = D_M + D_W$. Fig. 2.9 shows the dispersion curves of a conventional single mode fiber. By cancelling each other, the zero dispersion wavelength λ_{ZD} of a traditional single mode fiber is ~1.31nm. At λ_{ZD}, dispersion does not equal to zero and higher-order dispersion should be included into consideration. The dispersion slope $s = dD/d\lambda$ is responsible for the higher-order dispersive effects. The fiber loss is minimum near 1.55μm and D_W value could be changed by fiber design to shift λ_{ZD} to ~1.55μm. These fibers are referred to as dispersion-shifted fibers (DSF). For $\lambda < \lambda_{ZD}$, $D < 0$, fiber exhibits normal dispersion; for $\lambda > \lambda_{ZD}$, $D > 0$, optical fiber exhibits anomalous dispersion. The anomalous dispersion region has attracted many attentions in researching on nonlinear effects.

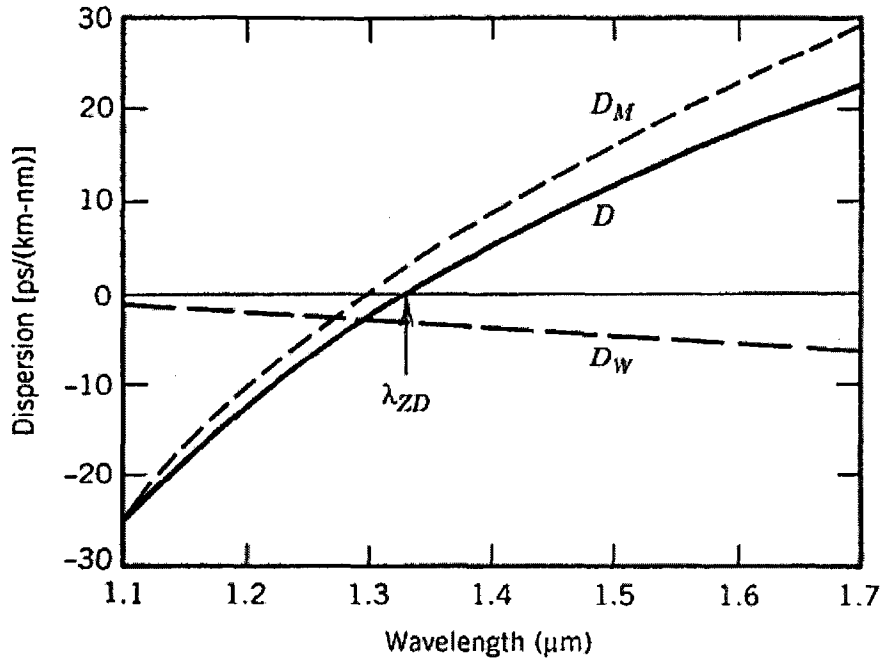

Figure 2.9: Material dispersion D_M, waveguide dispersion D_W and total dispersion D for a conventional single mode fiber from 1.1μm to 1.7μm wavelength range. λ_{ZD} stands for zero dispersion wavelength [35, 36].

- **Self-Phase Modulation (SPM) and Cross-Phase Modulation (XPM)**

At high intensity light, optical fiber behaves nonlinearly just like other materials. As a result, the refractive indices become power dependent and are given as [25]

$$n_j' = n_j + \overline{n_2}(p / A_{eff}), j = 1,2, \tag{2.4.1}$$

where j stands for core or cladding, $\overline{n_2}$ is the nonlinear-index coefficient, P is the optical power and A_{eff} is the effective area of the fiber. Due to the additional nonlinear term induced by $\overline{n_2}$ in Eq. (2.4.1), the propagation constant is rewritten as

$$\beta' = \beta + k_0 \overline{n_2} P / A_{eff} = \beta + \gamma P, \tag{2.4.2}$$

where $\gamma = 2\pi \overline{n_2} / (A_{eff} \lambda)$ is the nonlinear coefficient. And γ induces a nonlinear phase shift ϕ_{NL} that is given by

$$\phi_{NL} = \gamma P_{in} L_{eff}, \tag{2.4.3}$$

where L_{eff} is the effective interaction length defined as

$$L_{eff} = [1 - \exp(-\alpha L)]/\alpha \tag{2.4.4}$$

and α is the fiber loss. In a real laser diode, P_{in} varies with time and the time dependent phase results in the frequency shift $\delta\omega(t) = -d\phi_{NL}/dt$. Frequency shift $\delta\omega$ changes with time and this self-induced frequency chirp phenomenon is called self-phase modulation. The SPM-induced spectral broadening is shown in Fig. 2.10.

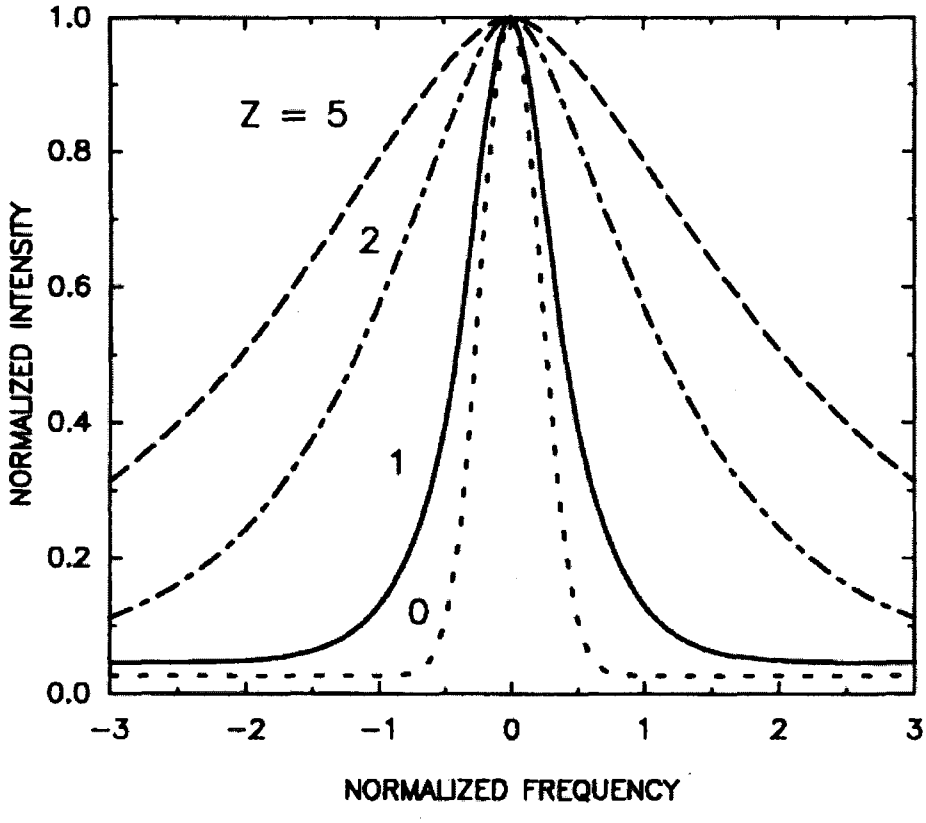

Figure 2.10: SPM induced spectral broadening of a CW beam as a function of propagation distance Z. The Z=0 curve corresponds to the input Gaussian beam [25].

XPM is another nonlinear phenomenon that results from the power dependence of the refractive index. The nonlinear phase shift depends on the power of two or more

optical fields that carry different frequencies. And the nonlinear phase shift of the *jth* channel is given by

$$\phi_j^{NL} = \gamma L_{eff}(P_j + 2\sum_{m \neq j} P_m) \tag{2.4.5}$$

- **Stimulated Raman Scattering (SRS) and Stimulated Brillouin Scattering (SBS)**

Spontaneous Raman scattering is an interaction between optical wave and silica molecules. During the interaction, the pump photon transfers part of its energy to the molecule in the vibrational state and emits in the form of a low-frequency photon. The frequency shifted light is called Stokes wave and is generated in all directions. If only pump propagates in the fiber, spontaneous Raman scattering could act as a probe to stimulate Raman Scattering and be amplified by SRS. The Raman–gain spectrum g_R as a function of the frequency difference between pump light and Stokes wave, Ω, is shown in Fig. 2.11. Note that g_R extends over a very broad wavelength range (~40THz) and maximum gain is at ~13THz. A higher-energy photon could also be created if the right molecule energy is added to the input photon energy. The generated wave is frequency up-shifting and called Raman anti-Stokes wave. The frequency shift is very small compared to the 13THz shift in the down-shifting process. Also, it is absorbed with increased pump and normally hardly observed in the amplification [31].

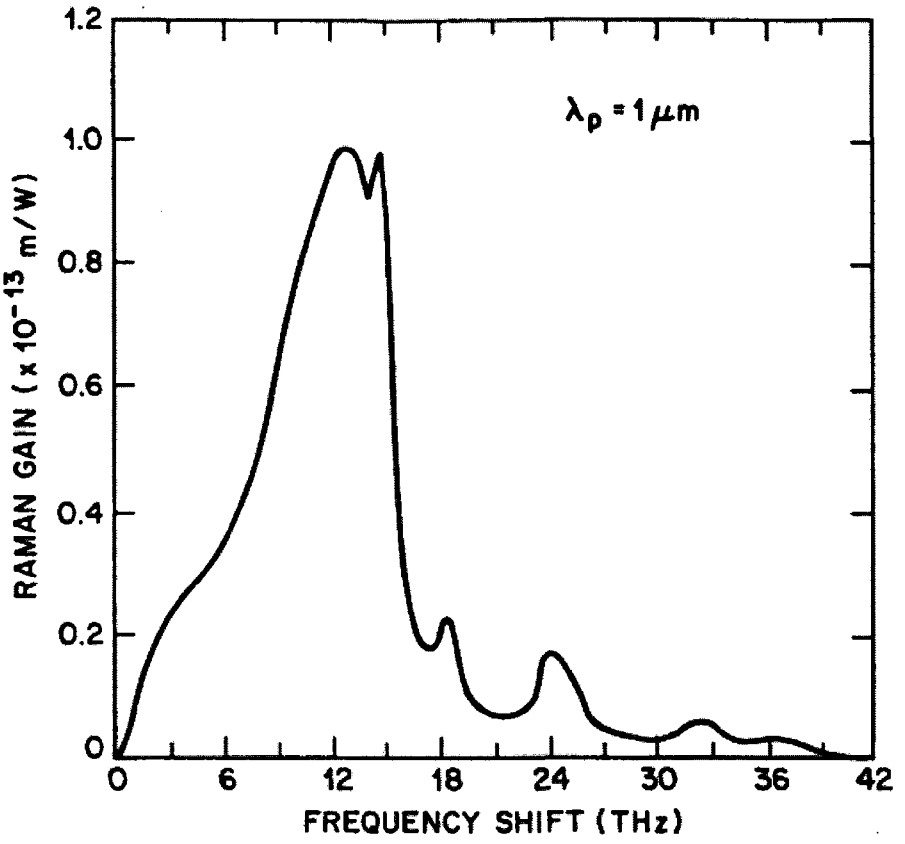

Figure 2.11: Raman gain spectrum of fused silica at pump wavelength of $\lambda_p = 1\mu m$ [25].

The threshold P_{th} for SRS is defined as the power of input pump at which the Stokes wave and the pump power have the same power at the fiber output and is estimated as

$$g_R P_{th} L_{eff} / A_{eff} \cong 16, \tag{2.4.6}$$

where g_R is the gain coefficient at the peak value, L_{eff} is defined in Eq. (2.4.4). If the pump wavelength is at ~1550nm and we use typical values of a single mode fiber in the formula, the calculated P_{th} is about 600mW [25]. It is much higher than the actual power used in the transmission that is below 10mW in one channel. Thus Raman scattering can hardly be observed in the single mode fiber. That is the reason that we use HNLF in the

experiment to reduce the threshold. Higher-order Raman Stokes lines will be generated once the power of the Stokes line is high enough to reach the threshold. In this way, pump power is transferred to long wavelengths side. Fig. 2.12 shows five Stokes lines generated by a 1-kW pulse pump. Power decreases towards higher-order Stokes lines but the gain peak becomes broader.

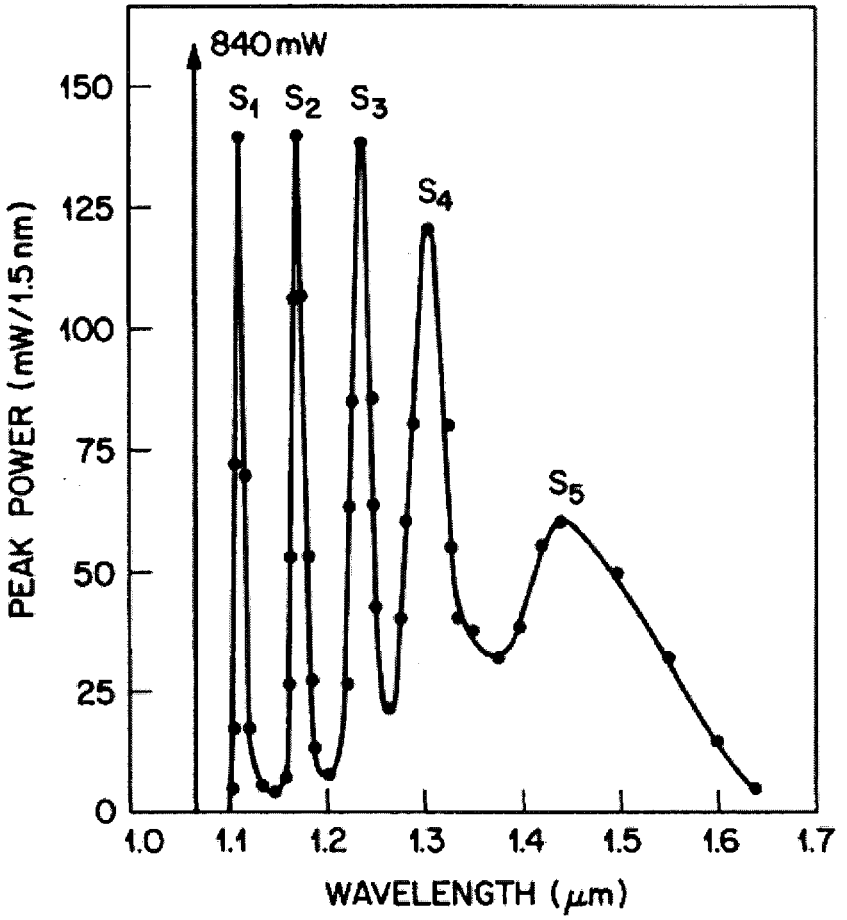

Figure 2.12: Cascaded Raman Stokes lines generated in the fiber [25].

SRS is very important in the SC spectral broadening due to the extremely broad amplification bandwidth.

SBS is another type of inelastic scattering. The differences between SBS and SRS are that the frequency shift in SBS is only about 10GHz and it occurs only in the backward direction. The threshold power P_{th} is approximately given by

$$g_B P_{th} L_{eff} / A_{eff} \cong 21, \tag{2.4.7}$$

where g_B is the SBS gain co-efficient and the typical value is ~100 times larger than g_R. The SBS threshold in the single mode fiber is only about 1mW. It removes light to the backward direction greatly once reaches the threshold and is detrimental for the system. It also inhibits SRS by carrying most of the input energy to the backward direction through Stokes wave. But the Brillouin gain is significantly reduced and the threshold is increased if the spectral width of the pump is comparable with the gain bandwidth (~10GHz). In our experiment, SBS can hardly be observed because the pumps are multimode and the ASE spectrum is broader than 10GHz.

- **Four-Wave Mixing (FWM) and Modulation Instability (MI)**

FWM is also originally from the nonlinear response of the medium to the optical light. But unlike SBS and SRS, the medium only plays a passive role. A wave at the new frequency ω_4 will be generated by three optical fields at frequencies ω_1, ω_2 and ω_3. These four frequencies are possibly to be formulated as following:

$$\omega_4 = \omega_1 \pm \omega_2 \pm \omega_3, \tag{2.4.8}$$

The net energy and momentum energy should be conserved to create new frequencies, which are referred as phase-matching condition. The relation $\omega_4 = \omega_1 + \omega_2 - \omega_3$ is relatively easy to occur that two photons of energies $\hbar\omega_1$ and $\hbar\omega_2$ generate two new photons with energies of $\hbar\omega_3$ and $\hbar\omega_4$ at frequencies ω_3 and ω_4.

And the total energy is conserved by $\hbar\omega_1 + \hbar\omega_2 = \hbar\omega_3 + \hbar\omega_4$. In this case, the phase-matching condition is relatively easy to be satisfied in the degenerate case when $\omega_1 = \omega_2$, $\omega_3 = \omega_1 + \Omega$, and $\omega_4 = \omega_1 - \Omega$, where Ω is the frequency difference. The phase-matching condition has three contribution parts: material dispersion Δk_M, waveguide dispersion Δk_W and nonlinear effects Δk_{NL}. They are given by

$$\Delta k = \Delta k_M + \Delta k_W + \Delta k_{NL} \tag{2.4.9}$$

$$\Delta k_M = [n_3\omega_3 + n_4\omega_4 - 2n_1\omega_1]/c \approx \beta_2\Omega^2, \tag{2.4.10}$$

$$\Delta k_W = [\Delta n_3\omega_3 + \Delta n_4\omega_4 - (\Delta n_1 + \Delta n_2)\omega_1]/c, \tag{2.4.11}$$

$$\Delta k_{NL} = \gamma(P_1 + P_2) = 2\gamma P_0, \tag{2.4.12}$$

where P_0 is the pump power and β_2 is the GVD coefficient and related to dispersion parameter D by $D = -\frac{2\pi c}{\lambda^2}\beta_2$.

In the single-mode fiber, contribution from waveguide dispersion is very small compared to the material dispersion except for very close to the zero-dispersion wavelength. The material dispersion part has to be negative to cancel the positive contribution from nonlinear effects. Thus, the pump light should be positioned in the anomalous dispersion region (D>0, $\beta_2 < 0$) and the phase-matching occurs at $\Omega = \pm\sqrt{\frac{2\gamma P_0}{|\beta_2|}}$. In the spectrum, two sidebands are amplified at frequencies $\omega_1 \pm \Omega$ as shown in Fig. 2.13. This phase-matching is realized by the nonlinear effects of SPM and is referred as modulation instability (MI). The frequency shifts by MI are in the range of 1-10THz for pump power ranging from 1-100W [25]. But the FWM induced spectral

broadening is much wider as illustrated in Fig. 2.14. The Raman Stokes line at ~13THz away from the pump wavelength is also observed in the output spectrum.

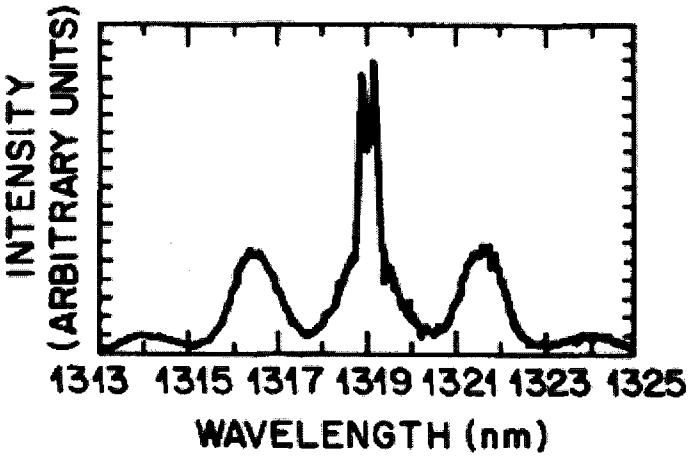

Figure 2.13: Spectrum illustration of side bands generated by MI effect [25].

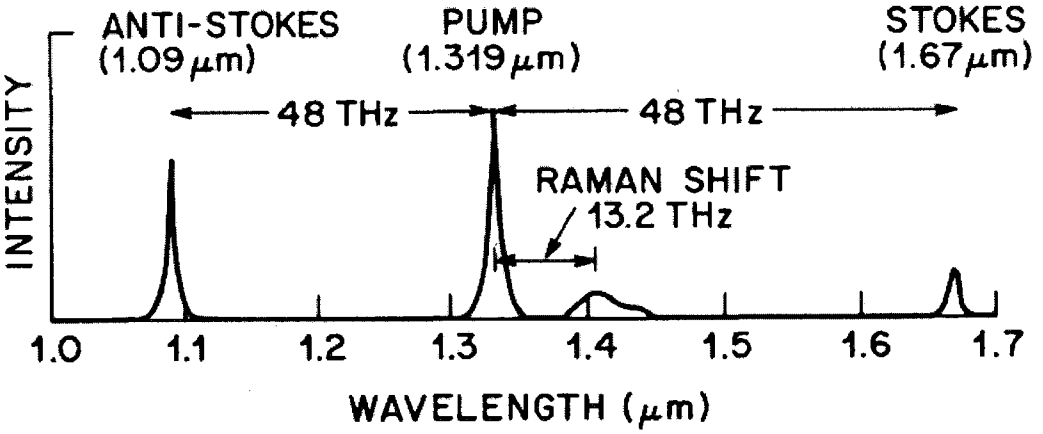

Figure 2.14: Stokes and anti-Stokes peaks generated by FWM effect pumped by a mode-locked laser with peak powers of ~1kW into a 50-m fiber [25].

2.4.2 Comparison of Single Mode Fiber (SMF), HNLF and Photonic Crystal Fiber (PCF)

- **Parameters of HNLF and SMF**

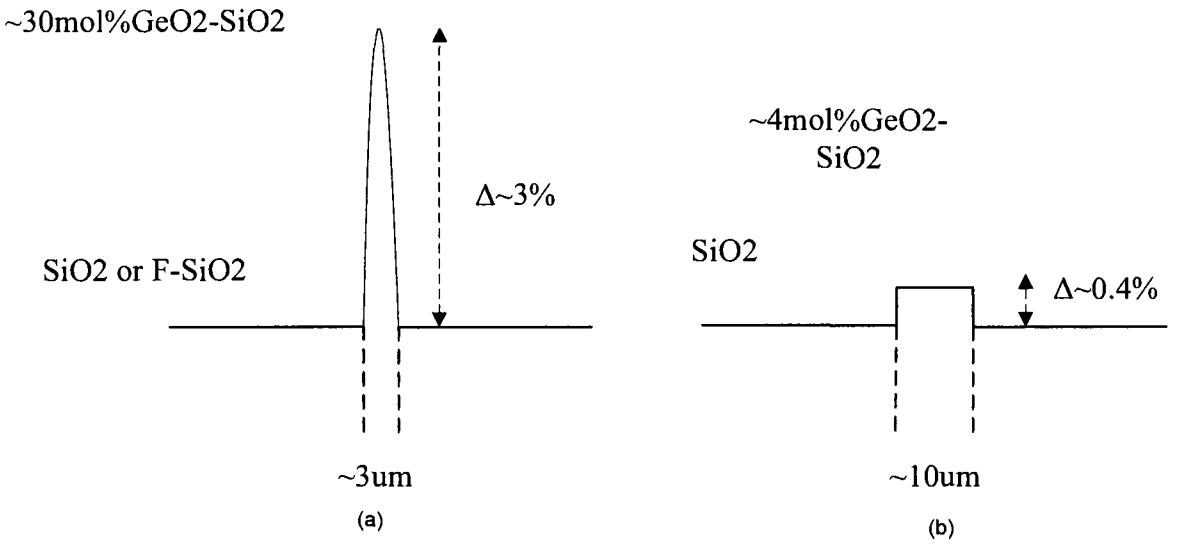

Figure 2.15: Refractive index profiles of (a) HNLF and (b) SMF [26].

Compared to the traditional SMF, HNLF has smaller core and higher refractive index difference Δ between core and cladding by doping with high germanium as shown in Fig. 2.15. Different fiber designs result in the high nonlinearity in HNLF as shown Table 2.2.

Table 2.2: Comparison of nonlinear parameters in HNLF and SMF [26].

Parameters	HNLF	SMF
Kerr coefficient(n_2)	$4-6(\times 10^{-20} m^2/W)$	$3(\times 10^{-20} m^2/W)$
Effective Area(A_{eff})	9-20(μm^2)	80(μm^2)
Nonlinear coefficient(γ)	10-30	1.5
Attenuation at 1550nm(α)	0.5-1(dB/km)	0.2(dB/km)
Zero Dispersion Wavelength(λ)	>1350(nm)	1310(nm)

The phase shift of SPM, threshold of SRS, side bands positions of MI in the Section 2.4.1 are all dependent on the high nonlinear coefficient γ, small effective area A_{eff} and high input power P_{in}. In Table 2.2, we find that these values are all optimized in HNLF compared to SMF. With high doping of *Ge* in the fiber core, Kerr coefficient n_2 is increased, although the fiber loss increases a little bit. The smaller A_{eff} value is obtained by fabrication of fiber with small core into which the light is confined. Higher n_2 and smaller A_{eff} values lead to higher γ in the fiber by the formula $\gamma = 2\pi\overline{n_2}/(A_{eff}\lambda)$. Thus nonlinear effects are greatly enhanced in the HNLF for spectral broadening.

- **HNLF and PCF**

As mentioned before, the specialty fiber with high nonlinearity used in generating supercontinuum spectrum is usually HNLF or PCF.

PCF is a micro-structured fiber with a small silica core surrounded by microscopic air holes. As seen from Fig. 2.16, the silica bridges between the air holes and core are very thin and the core is almost surrounded by air. Because of the refractive index difference between the core and the air-cladding, light is strongly confined to the small-size fiber core to provide high nonlinearity.

Also, the GVD profile of the fiber could be changed by modifying fiber structure, i.e., the sizes of core and cladding. Zero dispersion wavelength can even go to the green or near-infrared wavelength range, at which the conventional SMF is generally with normal dispersion value [31]. Usually, the possible zero dispersion wavelength of HNLF is longer than 1350nm and for PCF it is able to change from 700nm. Wavelengths of lasers for pumping also change according to the zero dispersion wavelength of the specialty fiber. An example is given in Fig. 2.17 [7]. The zero dispersion wavelengths of

the PCF and HNLF used are around ~800nm and ~1550nm. Thus two different lasers were taken as pumps. For broader continuum generation, pumping wavelengths should be placed in the anomalous-dispersion region [37].

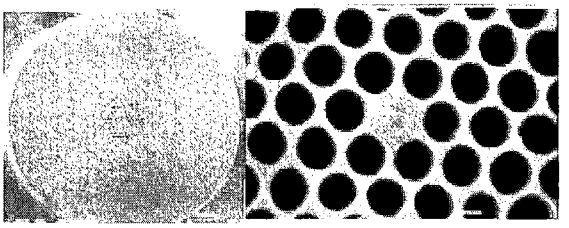

Figure 2.16: Micro-structure of PCF with centre solid-core and surrounding air holes [26].

PCF has offered a variety of new possibilities for efficient SC generation. It allows flexible dispersion profile through fiber structure modifications and provides high optical nonlinearities with the strong field confinement in small core of the fiber. As a result, the nonlinear-optical effects contributing to SC generation are significantly enhanced, which leads to highly efficient spectral broadening [39].

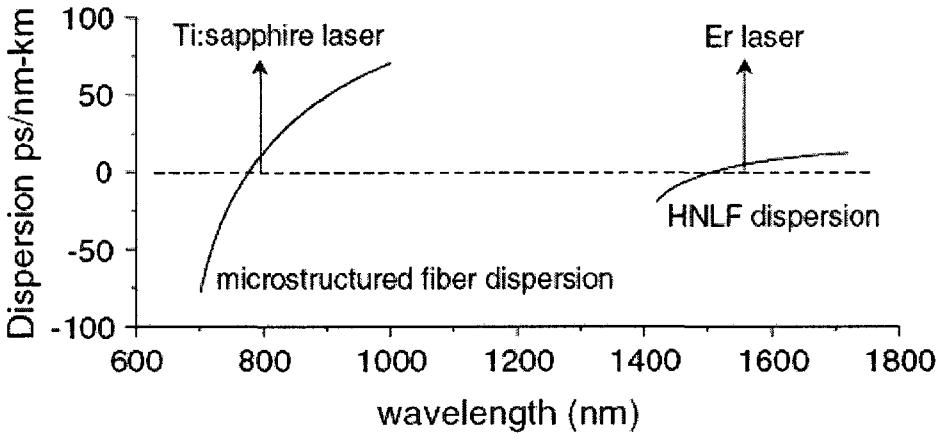

Figure 2.17: Comparison of dispersion curves for PCF and HNLF combined with input pulses[7].

The advantages and disadvantages of using HNLF and PCF are given in Table 2.3. Although PCF has higher nonlinearity than HNLF, it also has higher insertion loss.

In our experiment, ASE light before HNLF is around 1550nm and thus kilometer long HNLF is chosen as the nonlinear medium.

Table 2.3: Comparison between HNLF and PCF.

	HNLF	PCF
Advantage	• High nonlinearity: $10-30(W \cdot km)^{-1}$ • Splicing with low loss to SMF (0.2dB at 1550nm) • Low attenuation	• High nonlinearity: $10-100(W \cdot km)^{-1}$ • Flexible in controlling the dispersion profile • Short length required
Disadvantage	• Chromatic dispersion tailored within limited wavelength range	• High loss • Difficulty to manufacture

2.4.3 Three Types of HNLFs

In general, there are three types of HNLFs according to the applications. See Fig. 2.18 of their dispersion characteristics.

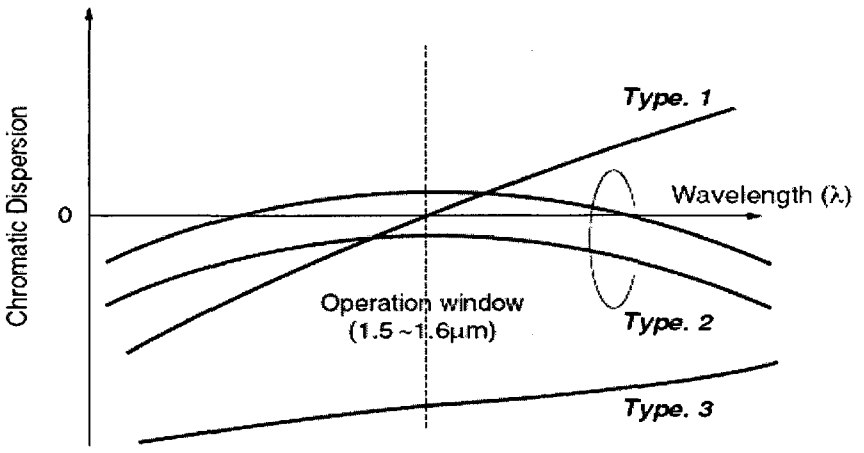

Figure 2.18: Dispersion characteristics of three types of HNLFs [27].

Type-1: Zero dispersion wavelength λ_0 is around 1550nm, and dispersion slope is positive and relatively large. This HNLF is mainly used for wavelength conversion or parametric amplification based on FWM or XPM. In Fig. 2.19, idler light, the newly generated light, is generated at output with one pump and one signal input. The frequency is Δf away from the pump light, which is the same as the frequency difference between the pump light and signal. The larger the Δf is, the lower power the converted light is [27]. And spacing between the pump wavelength and zero dispersion wavelength λ_0 is crucial in determining amplification bandwidth. Pump should be placed close to λ_0 and in the anomalous dispersion region (dispersion D>0) [37].

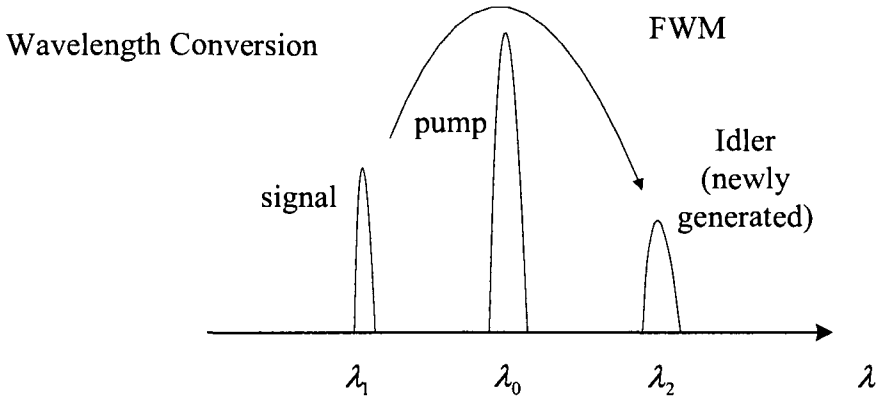

Figure 2.19: Illustration of wavelength conversion by FWM [27].

Type-2: Dispersion is almost zero across the transmission window 1500nm-1600nm. Fiber has low dispersion over a relatively large wavelength range (1.3-1.6μm). Dispersion slope *s* changes from positive to negative values within this range. It is similar to dispersion-flattened fiber and is referred as highly-nonlinear dispersion-flattened fiber (HNL-DFF). This kind of HNLF is suitable for supercontinuum generation as shown in Fig. 2.20. Many nonlinear effects occur and cooperate during such generation. By designing, the dispersion value can even decrease linearly along the fiber and is referred as dispersion flattened and decreasing fiber. It is expected to have better performance in the SC generation according to current research.

Supercontinuum Generation (SC)

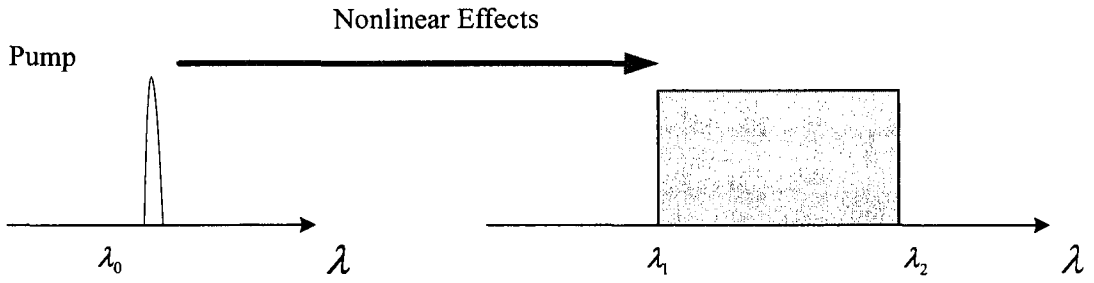

Figure 2.20: Generation of SC by nonlinear effects in the Type-2 HNLF [26].

Type-3 HNLF is for Raman amplification. As seen from Fig. 2.18, it has negative and big absolute dispersion value plus small dispersion slope around 1550nm. Phase-matching condition is hardly satisfied for FWM and MI. But with the low attenuation and high normalized Raman gain coefficient g_R / A_{eff}, as all HNLFs have in common, it is ideal for Raman effect. The parameter g_R / A_{eff} normally depends on the composition of the fiber core and varies with different doping in the core. Fig. 2.21 clearly shows remarkable contrast of the normalized Raman gain coefficient in different fibers.

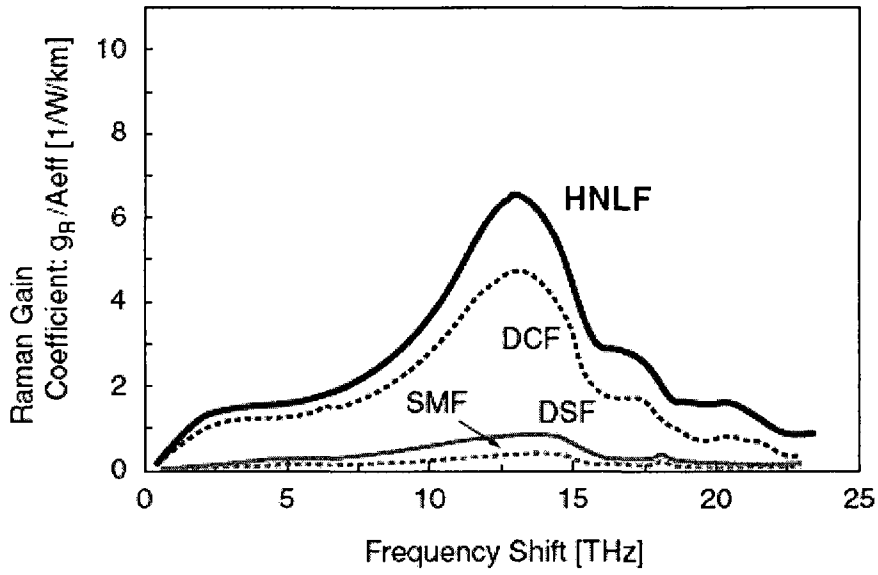

Figure 2.21: Comparison of g_R / A_{eff} in different fiber types for Raman effect [27]. SMF, DCF, and DSF stand for single-mode fiber, dispersion compensation fiber and dispersion-shifted fiber separately.

2.4.4 Two Units of HNLFs used in the Experiment

- **Dispersion and Nonlinear Parameters**

In our experiment, two units of HNLFs are used. Both HNLFs have kilometer lengths that are suitable for CW pumping. The technical parameters are shown in Table 2.4.

Table 2.4: Parameters of the two HNLFs used in the experiment.

Parameters		Unit-1	Unit-2
Length(m)		1210	2490
Cut-off wavelength λ_c (nm)		1550	1370
Nonlinear coefficient $\gamma(W \cdot km)^{-1}$		12(for random polarization state)	12(for random polarization state)
At 1550nm	Dispersion parameter D $ps/(nm \cdot km)$	-0.8	-12
	Dispersion slope s $ps/(nm^2 \cdot km)$	+0.03	+0.01
	Attenuation α (dB/km)	0.54	0.7
	$A_{eff}(\mu m^2)$	10	10
g_R / A_{eff} $(W \cdot km)^{-1}$		6.18	6.0
Fiber pigtail (both ends)		SMF	SMF
Connector (both ends)		SC/PC	SC/PC
Adaptor (both ends)		SC	SC

- **High Nonlinearity in the Fibers for SPM & SRS Effects**

As introduced before, many nonlinear effects take place in the spectral broadening. But their roles in each process are different that depend on the pump type and dispersion property of the fiber. As presented in Table 2.4, both of the two units of fibers have high nonlinear coefficient γ, small effective area A_{eff}, and low attenuation

α as well as long lengths. Thus they are both good media for spectral broadening induced by SPM and SRS which strongly depend on the nonlinearity as introduced in Section 2.4.1. For SPM, the maximum phase shift is given by Eq. (2.4.3), and in the case of intense ultrashort pulses, spectrum can be broadened over 100THz or more only by SPM because of the peak power [31]. Our two pumps are continuous wave where SPM plays a limited role compared to SRS, FWM and MI [7, 12, 32]. The physical mechanism for XPM is similar as SPM and is also limited in the CW pumping.

Unlike SPM, SRS does not depend on the pump type. It is an important effect in both pulse and CW pumping. Once threshold is reached, power will be transferred to long wavelength region continuously. The high values of g_R / A_{eff} and long lengths of our two HNLFs as shown in Table 2.4 greatly reduce the threshold for pumps and make them ideal for Raman amplification. Wide amplification bandwidth (up to 40THz) in the HNLF by cascaded SRS will extend spectrum to a very broad wavelength range. Strong SRS effect will be observed in our experimental results in the following two chapters.

- **Dispersion Properties for MI and FWM Effects**

Besides nonlinearity, dispersion parameter D and dispersion slope s at 1550nm are also provided in Table 2.4. Unlike SPM and SRS, the effects of FWM and MI not only depend on the fiber nonlinearity but also on dispersion values. Based on the dispersion values at 1550nm, the formula $D = S(\lambda - \lambda_0)$ is used to roughly estimate zero dispersion wavelength λ_0 and dispersion for the considered wavelength range.

For Unit-1: $-0.8 = 0.03(1550 - \lambda_0) \Rightarrow \lambda_0 = 1576.67nm$,

And for Unit-2: $-12 = 0.01(1550 - \lambda_0) \Rightarrow \lambda_0 = 2750nm$.

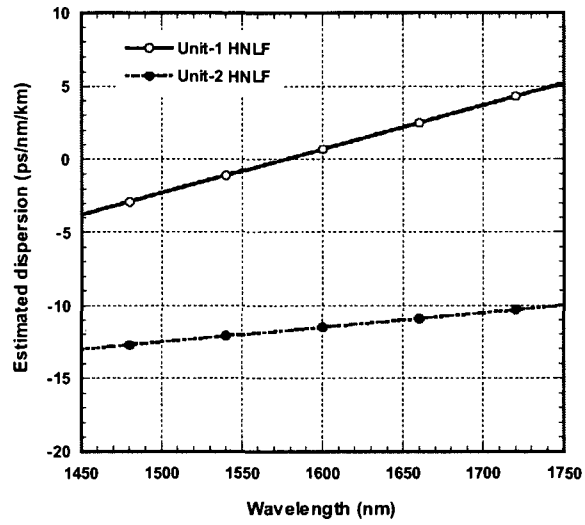

Figure 2.22: Estimated dispersion parameter versus wavelength for the two units of HNLFs.

Figure 2.22 depicts estimated dispersion parameter D versus wavelength for Unit-1 and Unit-2 fibers, respectively. The FWM and MI effects in the Unit-1 HNLF will be analyzed first. The zero dispersion wavelength λ_0 of the Unit-1 HNLF is at ~1576.67nm and the absolute dispersion value around 1550nm is small. The dispersion slope s is not large either. Although the peak of ASE from our EYDF is at ~1560nm, which will be shown in Fig. 2.24, its spectrum extends to more than 1600nm. Then part of its spectrum is in the anomalous dispersion region. These satisfy all the conditions for FWM and MI to occur. In the partially degenerate case in which $\omega_1 = \omega_2$ (MI), gain becomes maximum at the frequency shifts given by $\Omega_{max} = \pm\sqrt{\frac{2\gamma P_0}{\beta_2}}$. Large frequency shifts through MI is realized in the Unit-1 fiber with high nonlinear parameter γ and small dispersion value β_2. New frequencies generated by MI and SRS could also serve as pumps to generate new spectral components through FWM and extend spectrum to a much wider wavelength region. The closer the pump to the zero dispersion wavelength of HNLF, the

wider the amplification bandwidth and the more efficient the FWM effect we can get [27, 28].

J.W. Nicholson et al has demonstrated the importance of positions between pumping wavelength and zero dispersion wavelength in generating MI and FWM as shown in Fig. 2.23 [7]. The zero dispersion wavelength of the HNLF is ~1594nm. Two MI peaks are observed on the left graph when pumping at 1596nm. But no such peak appears on the right graph when pumping in the normal dispersion region at 1575nm. First-order Raman Stokes line is generated in both pumping conditions. Due to the pumping in the anomalous region, spectrum on the left graph is more broadened by MI and FWM compared to the graph on the right.

Then as for the Unit-2 HNLF, it has opposite dispersion values compared to the Unit-1 fiber at around 1550nm wavelength. The dispersion is normal ($D<0$) for the interested wavelength range, i.e. less than 2000nm. The absolute dispersion value is large but dispersion slope is small. This Unit-2 fiber was designed for Raman amplification only. MI and FWM rarely occur in the normal dispersion region. Thus the broadened spectrum is different that will be shown in our results.

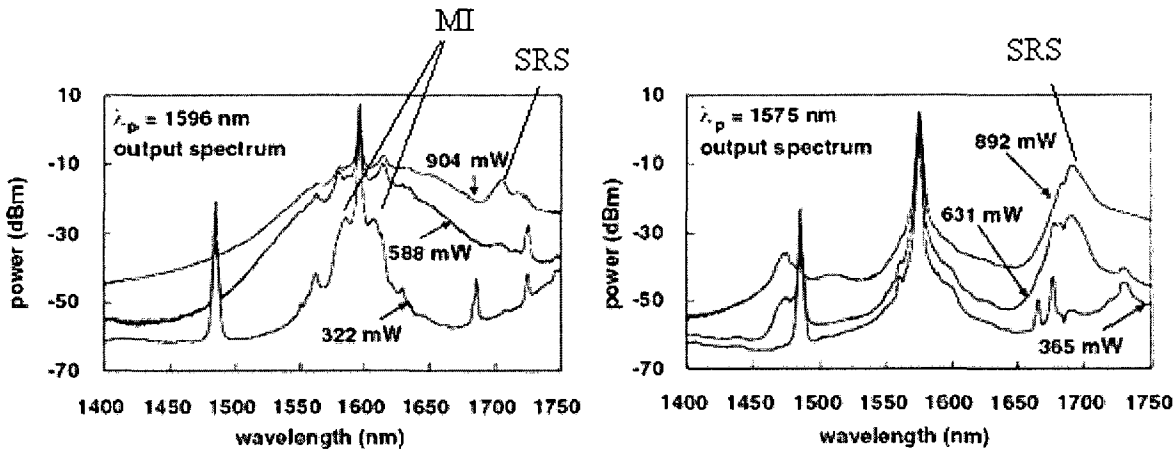

Figure 2.23: Illustration of MI effect at two pumping wavelengths. The zero dispersion wavelength is close to 1594nm. λ_p is the pumping wavelength [7].

In short, interaction of nonlinear effects in HNLF is able to generate supercontinuum when certain conditions are satisfied. SPM, XPM, SRS, MI and FWM are able to occur in the Unit-1 HNLF, while the last two effects hardly occur in the Unit-2 fiber. These two different HNLFs will be employed in our experiment to explore the roles of nonlinear effects.

2.5 Other Optical Components

2.5.1 Isolator

Optical isolator allows the transmission of light in one direction while blokes light in the other way. The benefits of an isolator are twofold: protecting lasers from back reflected light and guiding the light transmission in one direction in the ring. High power isolator of up to 3W is used in the experiment.

2.5.2 Splitter

Splitters are placed in the ring structure in Fig 2.1 as well as in the single line structure in Fig 2.2(b) to split the propagation light into two parts. In the ring structure, splitting ratios of 90:10, 80:20 and 50:50 are considered. Each splitter has its operation window. Most optical splitters are band limited devices. A broadband splitter usually has bandwidth of $\pm 40nm$ around the center wavelength, i.e. $1550 \pm 40nm$ in the experiment. Apart from the specified operation band, insertion loss increases a lot. The supercontinuum laser source has bandwidth of much wider than 100nm. Splitter bandwidth will limit the performance of the fiber ring laser in Fig. 2.1 in a certain degree.

2.5.3 Optical Spectrum Analyzer (OSA) and Power Meter

OSA is used to record spectrums in the frequency domain. The measurable wavelength is determined by the detector. Two OSA are used to record spectrums, ANDO AQ-6315A and Yokogawa AQ6375. Their measurable wavelength ranges are 350nm-1750nm and 1200nm-2000nm, respectively. The maximum input power is 100mW and light is attenuated before detecting.

Two power meters measure powers of different levels. Their spectral ranges are also limited by the detector. The one from Newsport could only detect light from wavelength of 640nm to 1600nm within 200mW optical power. And the high power meter from Gentec could detect optical light from wavelength of 190nm to 10μm within 30W.

2.6 Feasibility in Generating SC in the three Structures

2.6.1 Theoretical Basis

Pump type, pump power, pumping wavelength as well as zero dispersion wavelength of HNLF are crucial in SC generation. To economize our fiber laser, CW pumping regime other than short-pulse pumping is taken. In the CW pumping, compared to Raman fiber lasers (RFL), using multimode 975-nm pump lasers is considered as low cost. In the previous research on SC generation, at least Watt-level pumping is required under CW pumping. With RFL, usually at least one or two Watts are used in former experiments. RFL is pumped directly at desired dispersion wavelength based on the selected HNLF to broaden spectrum to supercontinuum and is highly efficient. But our multimode lasers are first pumped at 975nm and then transferred to desired wavelength (~1550nm) for SC generation through ASE. They are less efficient than RFL and thus higher power is required. Besides, in [17], SC is generated at 5.5W multimode pump level with 8m EYDF. But formed SC is only 53.4mW. Two pump lasers of altogether 12W are necessary for Watt-level SC. For high pump power to be completely absorbed, the length of co-doped fiber cannot be too short. Based on the experiment [17] that used 8-m long EYDF to absorb 5.5W pump, 15-meter EYDF in our experiment is a good choice for 12W pump. With 15-m EYDF, generated ASE is around 1550nm with gain peak at ~1564nm as shown in Fig. 2.24. And the zero dispersion wavelength λ_0 of the Unit-1 HNLF is estimated to be at ~1576.67nm. So ASE covers the anomalous dispersion region, which benefits for FWM and MI effects based on the above analysis. There is no restriction on light wavelength selection using Unit-2 HNLF due to its normal dispersion

property. Both of the two unit fibers are kilometer long, which are necessary for wide spectrum generation in the CW pumping regime. Kilometer lengths are always required in CW pumped SC [29, 30, 33, 34] with HNLF, while with short pulses, a few meters long is generally enough [7]. CW light have low peak to average power ratio compared to short pulses so long interaction lengths are necessary. Moreover, the generated ASE is broadband and its bandwidth exceeds spectral width of the Brillouin gain, which prevents backward propagating light by SBS. In short, each component performs its own role and contributes to SC generation as a whole.

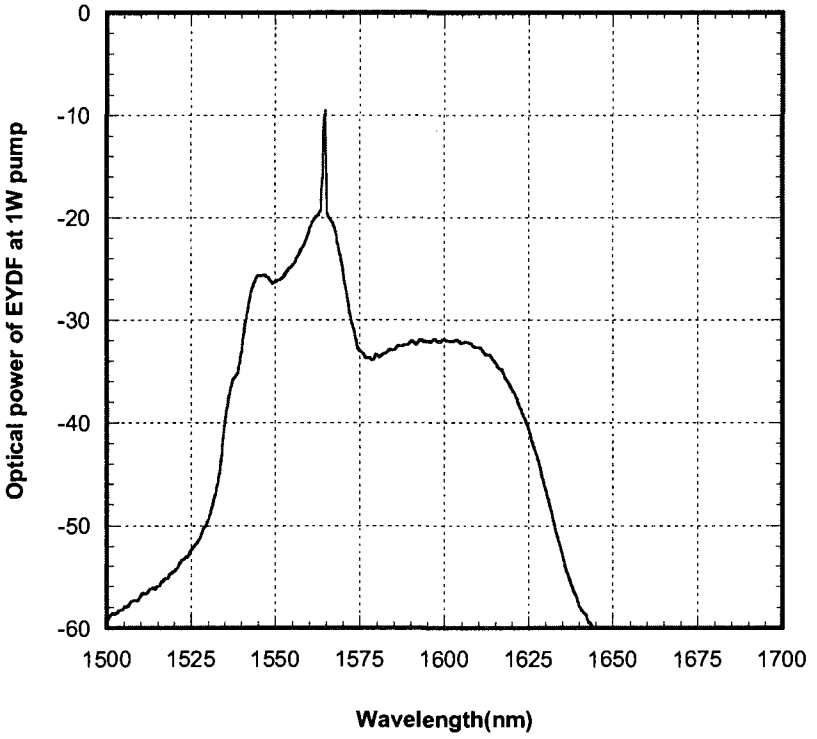

Figure 2.24: Spectrum of forward ASE from EYDF at 1W pump.

2.6.2 Connections between Components

Except for theoretical feasibility, practical operation is also concerned. For the setup to work well for efficient SC generation, connection between two components is

essential to ensure low loss and stability. To couple light from one component to the other, usually two methods can be adopted: splicing fiber pigtails together or using connectors. Our pump lasers and combiner are ordered with ~1m pigtail while SC/PC connectors are provided in the two units of HNLFs.

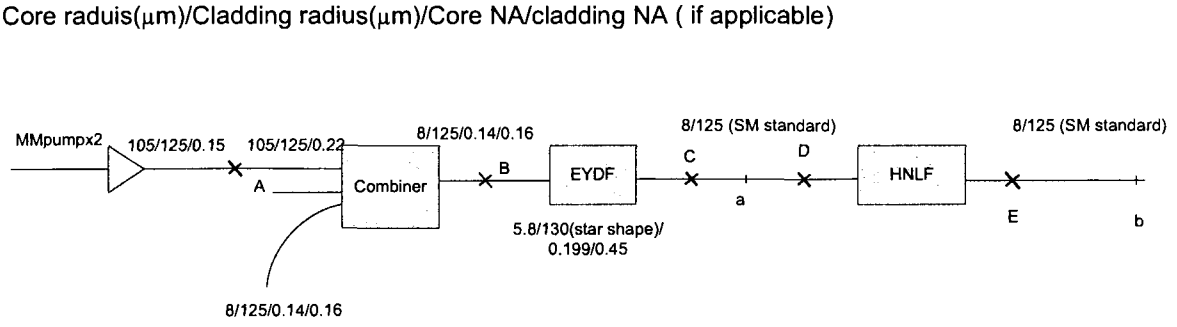

Figure 2.25: Diagram illustration of connection between components.

Figure 2.25 illustrates connections between each two components in our experiment. Letters A, B, C, D and E stand for connections with splicing. Letters a and b represent connections using SC/PC connectors. SC/PC is one commonly used connector type. To ensure low loss connection, fiber and connector of the same type are preferred. We selected the components to ensure the compatibility of fiber pigtails. Usually three values are given for a fiber pigtail: core/cladding diameters and NA. Fiber with large NA has better light coupling capacity. In DCF, EYDF and two ports of the combiner, light propagates in both core and cladding and two NAs are provided. The fusion splicer of Sumitomo T-36 is used for splicing in the experiment. We use stripper to get rid of the coating on the fiber (the second cladding), clean with 99% isopropyl alcohol and Lint-free wipes, cut vertical and flat fiber end with cleaver and then insert them immediately into the groove of the fusion splicer for splicing. The splicing loss is around

0.01dB for the same type of fiber. Good splicing is required to ensure stability of light propagation as well as accurate results especially in the high power operation. Figure 2.26 shows one burned connection due to bad splicing.

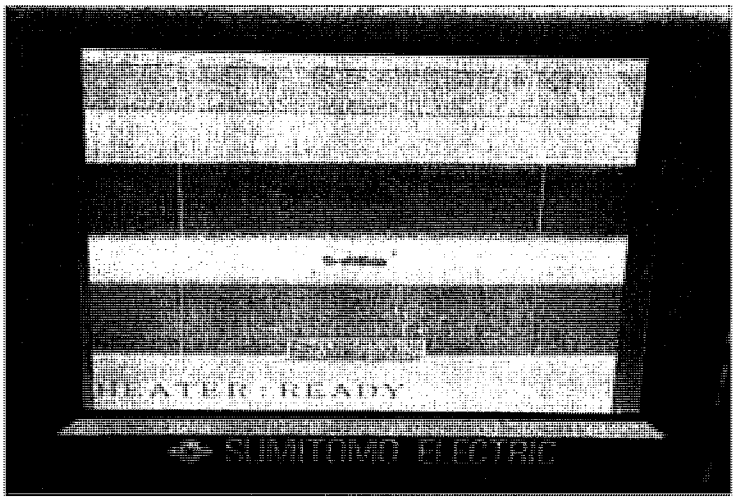

Figure 2.26: Illustration of two burned spliced fiber pigtails at the splicing point.

For HNLF, the core area is very small and specific splicing machine and techniques are required to splice the small-core fiber to SMF to achieve low loss. So for each unit, the two ends are already spliced to single mode fiber pigtails by the producer. Typical splice losses for SMF to HNLF are 0.2dB at 1550nm. The other end of the SMF pigtail is SC/PC connector with adapter. Two connectors of the same type should be inserted into the adapter to align the fiber cores as to pass light with low loss. Under high power, connectors have to be very clean to avoid burning.

CHAPTER 3 CW PUMPED SC FIBER RING LASER

In this chapter, experiment results obtained in the first design in Fig. 2.1 will be presented. In this ring structure, output power from HNLF is separated into two parts via a fiber splitter.

Firstly, evolution processes of SC formation in the ring structure will be shown and the effect of splitting ratios on the SC spectrum as well as output optical power will be investigated. Splitter ratios of 90:10, 80:20 and 50:50 are taken in the ring structure. For the ratio 90:10 (or 80:20), two cases are considered, by taking 90% (or 80%) and 10% (or 20%) as output optical power. Spectrums above are recorded with OSA of ANDO AQ-6315A and resolution of 0.05nm is used.

Next, the splitter ratio is fixed at the optimum splitting value. And by inserting Unit-1, Unit-2 HNLF and their combinations (Unit-1+Unit-2 and Unit-2+Unit-1) into the ring, the impact of nonlinear effects, i.e. SPM, XPM, MI, SRS and FWM on the CW based SC generation is further investigated. Note that the two units of HNLFs have different GVD and zero-dispersion wavelengths.

3.1 SC Generation with 90(out):10(in) Splitting Ratio in the Ring Structure

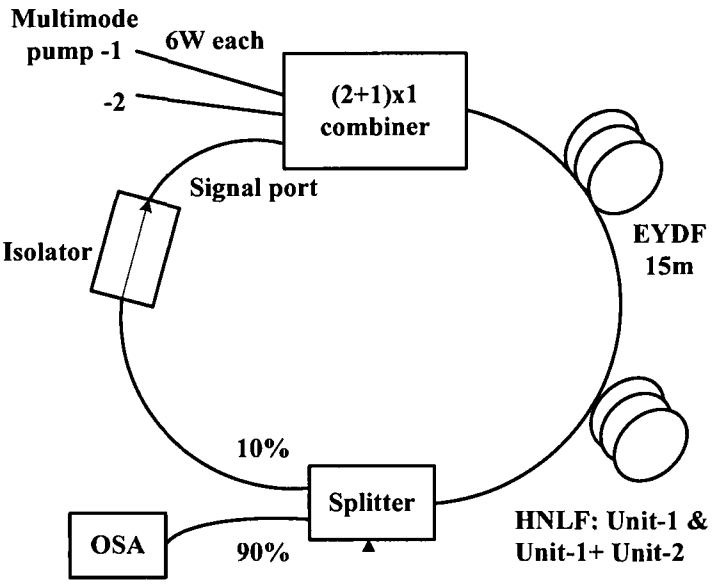

Figure 3.1: Illustration of the fiber ring laser with splitting ratio of 90:10. The 90% portion light is taken as output and 10% part is fed back to form the ring.

3.1.1 Optical Spectrum Evolution

As presented in Fig. 3.1, splitting ratio of the splitter is 90:10, where the 10% portion of the light is fed back into the ring laser and the remained 90% portion of the light is taken as output. Fiber Unit-1 and the combination of Unit-1+Unit-2 are inserted into the ring cavity. The Unit-1 fiber is first used in the ring. Figure 3.2(a) shows the evolution of optical spectrum versus wavelength with a parameter of pump power at 975nm, where the pump power of 1, 2.6, 4, 6, 7.6 and 9W is considered. When the pump power is 1W, an optical peak is observed at ~1567nm. This peak is formed by the ASE in the EYDF and broadened by SPM. With pump power increased to 2.6W, another peak at

~1616nm appears. It is worth mention that this second peak also exists without the HNLF but with much lower power. Indeed, this peak is originated from the long fiber ring cavity and further amplified by SRS in the HNLF. Its broadness can also be attributed to SPM. Also at this pump level, about ~13THz away from the 1567nm peak, a first-order Stokes line induced by SRS emerges at ~1670nm. In addition, a small peak at ~1526nm is observed to appear on the left side of the 1567nm peak. This peak and the ~1616nm peak are both ~5THz away from ~1567nm and are considered as MI peaks. Compared to Fig. 2.13, the asymmetry of the two MI peaks is caused by SRS effect. When power increases to 4W and 6W, the double peaks at 1567nm and 1616nm keep increase in power and broadness. Spectrum extends towards both short and long wavelength regions by the effects of SPM, XPM, SRS, MI, and FWM. At 7.6W pump, the ~1616nm peak suddenly decreases and becomes flatter by transferring power to other parts of the spectrum through nonlinear effects. At the same time, a broadband continuum from 1450nm to 1750nm is formed. The spectrum hardly changes when pump increases from 7.6W to 9W. Optical output power of the formed SC is about 933mW. The spectrum has two major peaks from the EYDF and the ring structure, and all other parts show flatness. The amplification asymmetry in the two regions separated by the two peaks is obviously caused by SRS, which transfers power from short to long wavelength side continuously with its wide amplification bandwidth.

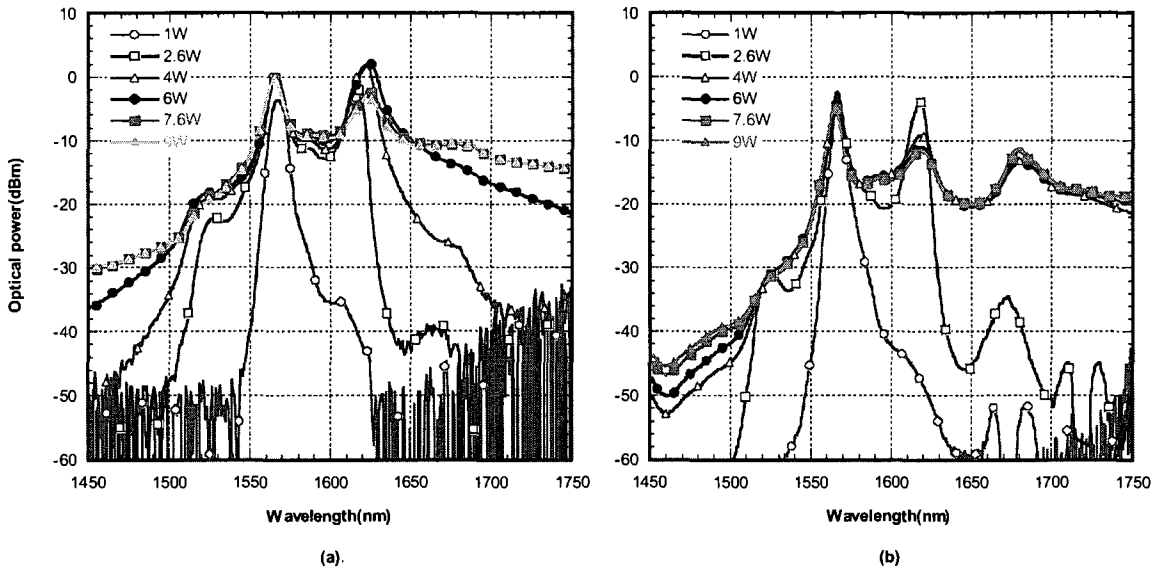

Figure 3.2: Optical spectrum versus wavelength with a parameter of 975-nm pump power using a 90:10 splitter and (a) Unit-1 fiber, (b) Unit-1+Unit-2 fiber in the ring structure.

Now the Unit-2 fiber is inserted in the ring structure after Unit-1, i.e. Unit-1+Unit-2. Figure 3.2(b) exhibits the result in terms of wavelength versus optical power. The evolution process is similar as in Fig. 3.2(a), where two major peaks emerge and grow with the increase of the pump power. The spectrum extends towards both wavelength sides under the interaction of many nonlinear effects too. But the first-order Raman peak at ~1670nm is more obvious in the formed SC compared to the one in the 1-km (Unit-1) SC. And the spectrum in the shorter wavelength region is less amplified. These are due to strong Raman effect in the Unit-2 HNLF. Since long HNLF provides long interaction length for nonlinear effects, SC is formed at lower pump power of 4W whereas with only Unit-1 fiber the critical pump power for the SC generation is 7.6W. Output optical power of formed SC in Fig. 3.2(b) is only ~268mW due to additional attenuation loss in the Unit-2 fiber.

3.1.2 Comparison between SC Generated with Unit-1(1km) and Unit-1+Unit-2 (1km+2km) HNLF

Wider SC spectrums from wavelength of 1200nm to 1750nm at 9W pump for Unit-1 and Unit-1+Unit-2 HNLF are shown in Figure 3.3. Both of the spectrums smoothly extend from wavelength of 1300nm to 1750nm. The higher SC spectral level is obtained in SC with only Unit-1 HNLF in the ring, for the whole wavelength region. A big valley is observed in the spectrum between 1400nm and 1500nm in the SC with two spools of HNLFs. Because Raman effect down-shifts frequency, amplification in the normal dispersion wavelength region is mainly by FWM (including MI) when pumping in the anomalous region in our case. This big valley is in the normal dispersion region and is an indication of deficiency of FWM and MI effects and very strong SRS.

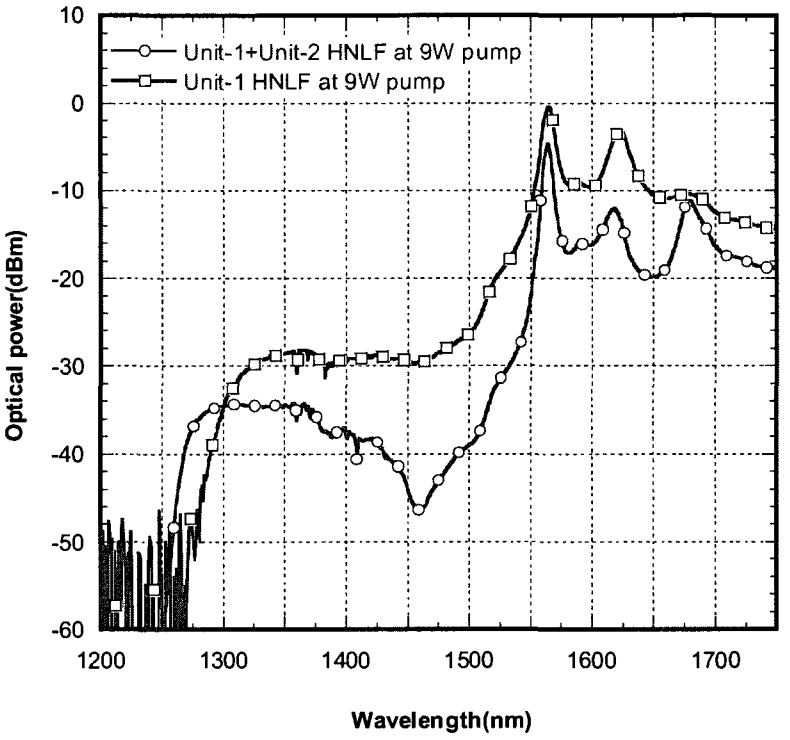

Figure 3.3: Generated SC spectrum from 1200nm to 1750nm with Unit-1 HNLF (blank square) and Unit-1+Unit-2 HNLF (blank circle)

3.1.3 Output Optical Power

In addition to the spectrum, Fig. 3.4 gives the output optical power as a function of pump power corresponding to the two SCs in Fig. 3.2(a) and (b). The 10% fed back light in the ring is gradually amplified by EYDF until stable. In both cases, output power of the continuum grows very fast at low pump powers. In the SC with Unit-1+Unit-2 HNLF, output power suddenly decreases when pump power increases from 3.6W to 4W. This indicates that the spectrum might have extended to longer and high loss wavelength region after 1750nm at 4W pump by power transfer from the ~1616nm peak in Fig. 3.2(b). It is not within the measurable wavelength of the ANDO AQ-6315A OSA, which is from 350nm-1750nm. Broader spectrum with the OSA of Yokogawa AQ6375 will be

shown later (with measurable wavelength from 1200nm-2000nm). Because the spectrum extends to both wavelength sides gradually with increased pump power in Fig. 3.2(a), there is no such power decrease in the SC with only Unit-1 HNLF. But the growth speed of the SC power becomes slow at high pump powers. And when SC is formed, not only the spectrum but also the output optical power hardly change.

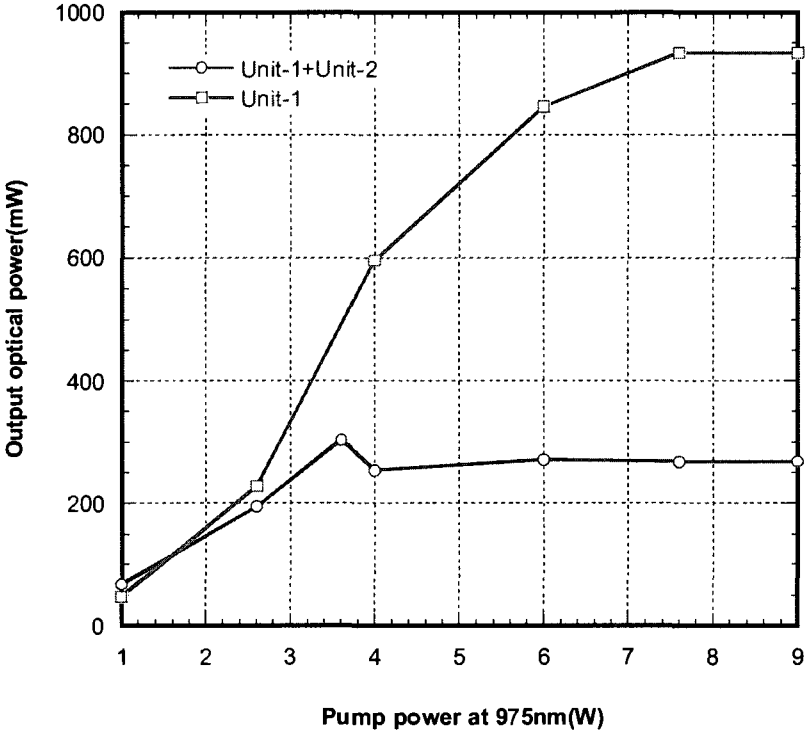

Figure 3.4: Output optical power of the SC versus pump power at 975nm with Unit-1 HNLF (blank square) and Unit-1+Unit-2 HNLF (blank circle)

Table 3.1 concludes spectrums and output powers of the formed two fiber ring lasers from the above three figures.

Table 3.1: Comparison of SC properties generated in the Unit-1 and Unit-1+Unit-2 HNLF

Type of HNLFs in the ring	SC coverage		Output power	Critical pump power
	20-dB	30-dB		
Unit-1+Unit-2	200nm 1550-1750nm	235nm 1515-1750nm	268mW	4W
Unit-1	230nm 1520-1750nm	430nm 1320-1750nm	933mW	7.6W

As seen from Table 3.1, the formed SC has better spectrum coverage as well as much higher optical power with only Unit-1 HNLF in the ring. The 30dB bandwidth is about 200nm wider and output power is close to Watt level. Although the 20dB bandwidth is not very wide, the spectrum is separated into two flat parts except for the two peaks in the centre. In the SC with Unit-1+Unit-2 HNLF, 4W pump power at 975nm is able to generate continuous spectrum which could save one multimode pump laser. However, HNLF is much more expensive than the multimode laser. Thus, with 90(out):10(in) splitting ratio in the ring, SC formed with 1km (Unit-1) HNLF has better performance and is preferable economically and practically.

3.2 SC Generation with 90(in):10(out) Splitting Ratio in the Ring Structure

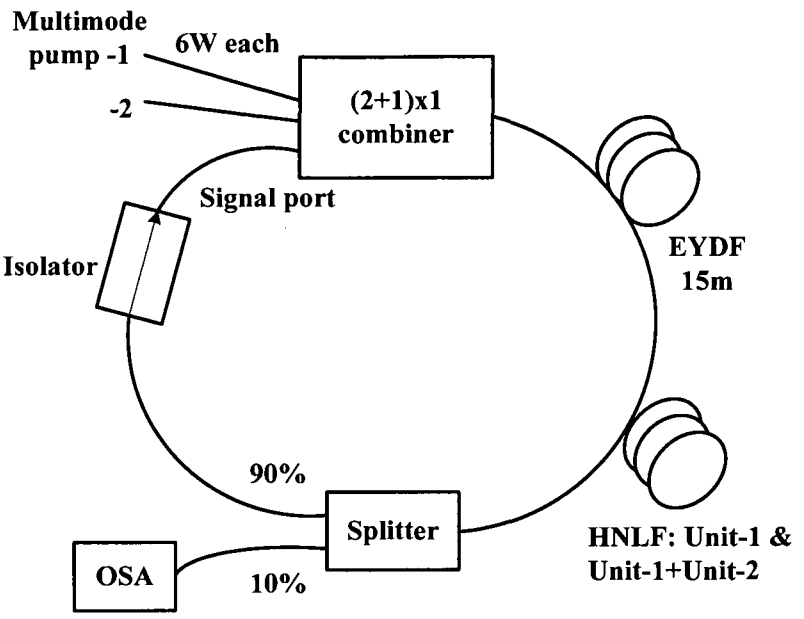

Figure 3.5: Illustration of the fiber ring laser with splitting ratio of 90:10, where the 90% part is fed back into the ring and the 10% light is taken as output.

In the above discussion, splitter of the 10% portion light is fed back to form SC. Now the 90% ratio light is fed back to the ring and the 10% part is taken as output to see the spectrum and output power of SC, as shown in Fig. 3.5. Other components in the setup remain the same.

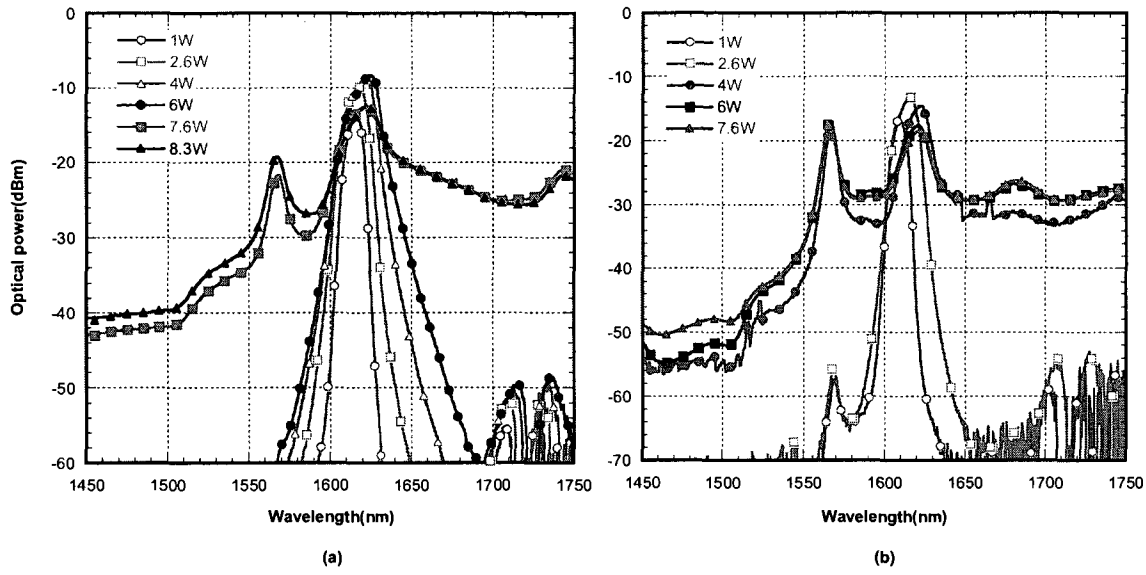

Figure 3.6: SC evolution with increased pump power using 90(in):10(out) splitter with (a) Unit-1 HNLF and (b) Unit-1+Unit-2 HNLF.

Figure 3.6(a) and (b) exhibit the generated continuum with increased pump power by inserting Unit-1 and Unit-1+Unit-2 HNLF into the ring separately. SC from 1450nm to 1750nm is also generated with this splitting ratio in both Unit-1 and Unit-1+Unit-2 HNLFs. Evolution processes and SC shapes are almost identical as former ones as the same nonlinear effects are involved. The double peak characteristic is still remarkable in the SC which confirms our deduction that it is caused by the ASE in the EYDF and the ring structure. However the peak at ~1616nm experiences more gain than the ~1567nm peak here. Note that in Fig 3.6(a), when the pump power increases from 1W to 6W, the ~1616nm peak grows and is broadened while the ~1567nm peak is hardly observed. In Fig 3.6(b), the peak at ~1567nm is also small at low pump power of 1W and 2.6W. Due to the deficiency in amplifying the large ratio feedback light (90%), Er ions are more likely to be excited to the lower state level at ~1616nm. And in Fig 3.6(a), only the first Stokes wave at ~1744nm, induced by the 1616nm peak, is observed at 7.6W and 8.3W pump due to the higher gain at 1616nm.

Spectrum comparison is given in Fig 3.7. Spectrums are also separated into two parts by two peaks. Both SC spectrums are asymmetric, which is due to the Raman effect. The 20dB bandwidths in Fig. 3.7 (a) and (b) are 220nm in wavelength, from 1530nm to 1750nm and 200nm, from 1550nm-1750nm separately. Higher spectral level on OSA is observed with 1km Unit-1 HNLF in the ring in the whole amplification band, the same as Fig. 3.3. As seen from Fig. 3.8, output optical power is only ~10mW, which is much lower than the ring formed with the 10% fed back light. It increases with pump power and suddenly decreases from 22mW to 14mW when SC is formed at 7.6W (Unit-1 HNLF) and from 19mW to 12.5mW at 4W pump (Unit-1+Unit-2 HNLF). This also indicates spectral extension to wavelengths longer than 1750nm. In this 90% fed-back ring, the SC still has better performance with only Unit-1 HNLF in the ring, i.e. higher output power and broader 20dB bandwidth, although not that remarkable compared to the 10% fed back ring.

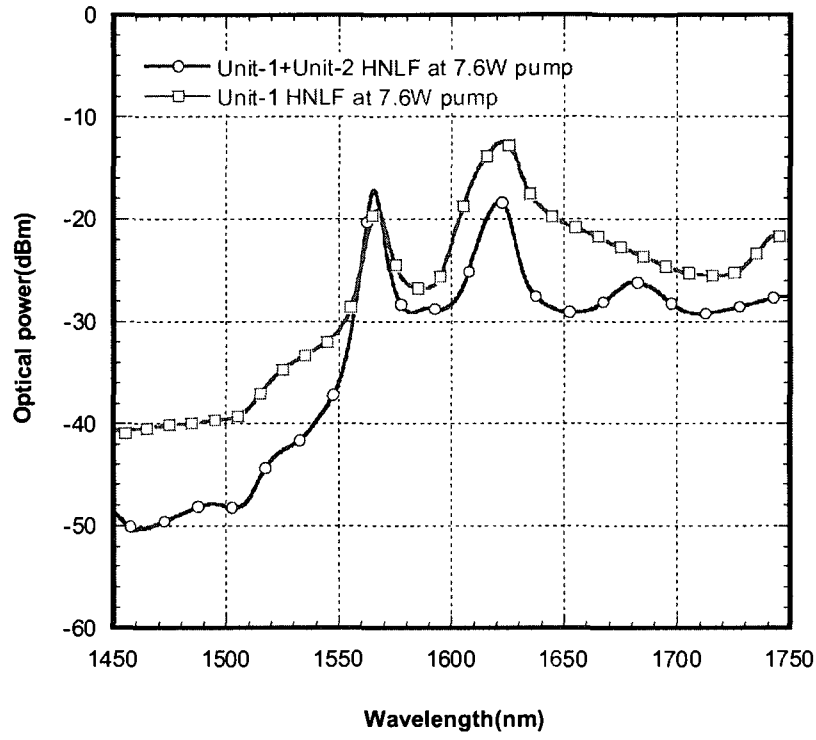

Figure 3.7: Comparison of formed SC with Unit-1 (blank square) and Unit-1+Unit-2 (blank circle) HNLF.

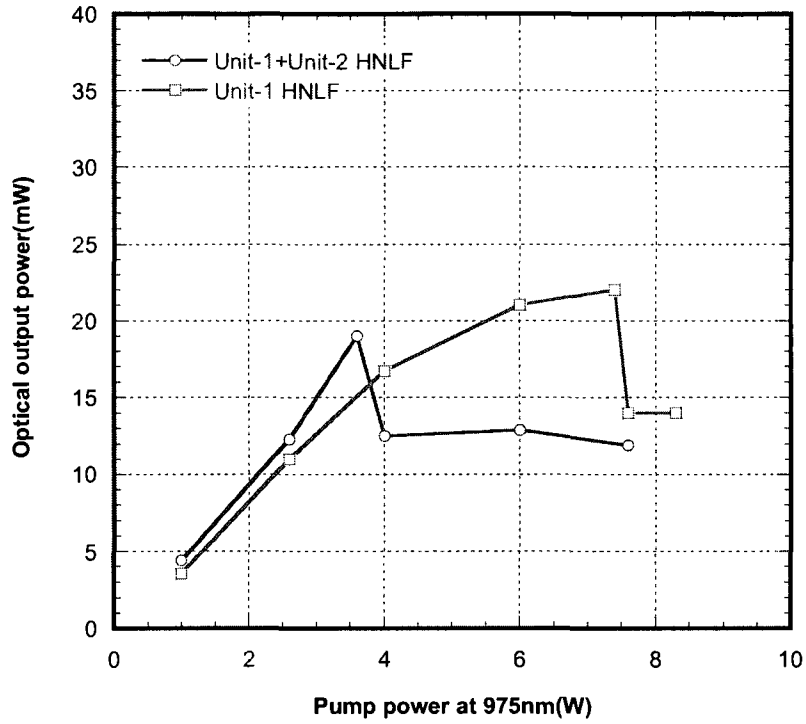

Figure 3.8: Output optical power of SC as a function of pump power at 975nm with Unit-1 HNLF (blank square) and Unit-1+Unit-2 HNLF (blank circle) in the ring.

3.3 Effects of Splitting Ratios on the SC Generation in the Ring Structure

The splitter ratios in the ring are changed to 80:20 and 50:50, and the above steps are repeated to see the changes. Figure 3.9 shows formed six SCs combining three splitting ratios and two HNLFs. Broadband continuums are successfully generated in all combinations of splitting ratios and HNLFs. It is found that the change of splitting ratio almost has no impact on the shape and broadness of the continuum but it plays an important role on the SC output power. Output optical power decreases when less portion of light is taken as output, which is understandable. For all splitting ratios used in the ring, flatter spectrums and higher spectral densities are observed when only Unit-1 HNLF is inserted into the ring. And with Unit-1+Unit-2 HNLF in the ring, there is always a big

valley around 1450nm and the first-order Raman Stokes line at ~1670nm is also clearer, which destroys the smoothness of the spectrum a lit bit.

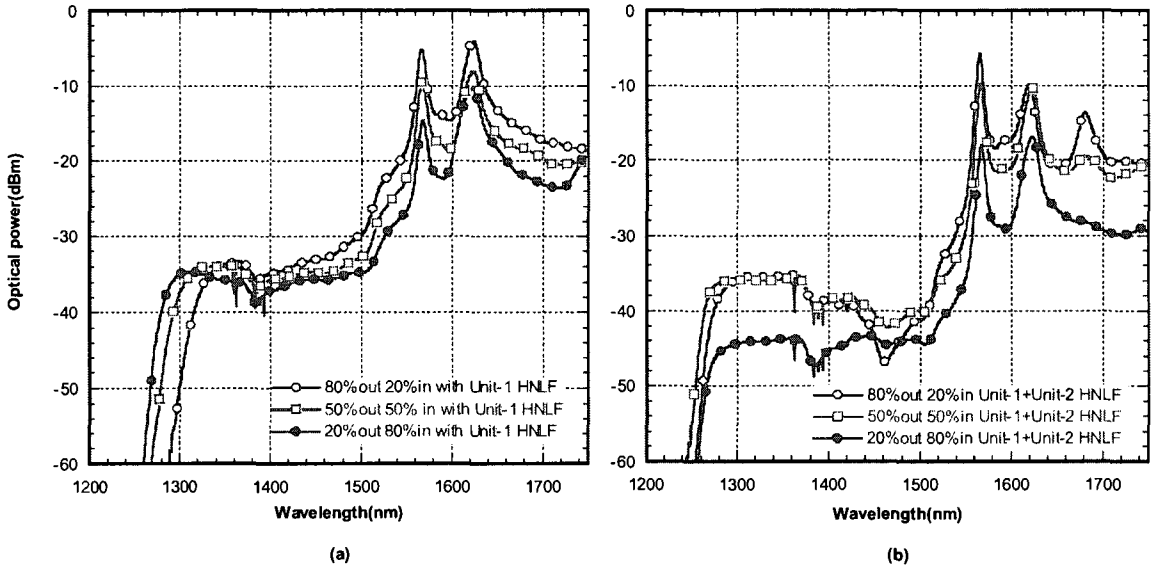

Figure 3.9: SC spectrum with (a) Unit-1 HNLF and (b) Unit-1+Unit-2 HNLF by using splitting ratios of 80:20 (blank circle), 50:50 (blank square), 20:80 (solid circle) in the ring.

Table 3.2 lists important parameters regarding spectrums and powers of the formed SCs. Due to the high gain at two peaks, 20-dB bandwidths are only ~200nm. But almost no spectral fluctuation is observed from 1300nm to 1500nm and from 1630nm to more than 1750nm with Unit-1 HNLF in the ring. By combining Table 3.1 and Table 3.2 and considering spectrum coverage, output power and cost, the optimum scheme is to use 90:10 splitting ratio, take 90% portion light as output and insert only Unit-1 HNLF into the ring.

Table 3.2: Comparison of SCs formed with eight splitting ratios in the ring structure

HNLF Type	Splitting Ratio (out: in)	20dB SC Coverage	Output Power
Unit-1+Unit-2	80:20	200nm(1550-1750nm)	263mW
	50:50	200nm(1550-1750nm)	183mW
	20:80	205nm(1545-1750nm)	35mW
	10:90	200nm(1550-1750nm)	11.9mW
Unit-1	80:20	235nm(1515-1750nm)	739mW
	50:50	230nm(1520-1750nm)	402mW
	20:80	225nm(1525-1750nm)	121mW
	10:90	220nm(1530-1750nm)	14mW

3.4 Wider Optical Spectrum Observation and Roles of Nonlinear Effects under CW Pumping

As discussed in Section 3.3, the best SC is obtained with splitting ratio of 90:10 in the ring, when the 90% light is taken as output and the 10% light as feedback. It will be demonstrated in this section that the SC indeed extends to the wavelength band of longer than 1750nm at high pump power and covers an optical spectrum from 1300nm to 2000nm by using OSA of Yokogawa AQ 6375 and taking 1nm resolution.

It has been shown that many nonlinear effects in the fiber are involved in the optical SC generation and development, such as SPM, XPM, SRS, MI and FWM. As introduced before, for the ultra-short pulsed laser pumped SC such as femtosecond pulses, the ultra-short pulses have very high peak power and thus the SPM effect has

significant impact on the broadening and flatness of the SC generation. And for CW pump laser based SC generation, the SRS and FWM (including MI) effects are the main reason for the SC generation where the SPM effect is very limited. SRS has already been proved to be very important for SC generation in the previous research due to the wide amplification bandwidth (~13THz). It is also clearly observed in our experiment as the asymmetric spectrum is always found in the formed SC. It is known that FWM effect significantly depends on phase matching that is dependent on the group velocity dispersion (GVD) of the specialty fiber. In other words, GVD characteristic of the fiber plays a critical role in the CW pump laser based SC generation. Different HNLFs of Unit-1 and Unit-2, with normal and anomalous dispersion properties at ~1550nm, and their combinations are employed in this section to further investigate the roles of nonlinear effects especially FWM on the broadness and flatness of the generated SC, as shown in Fig. 3.10.

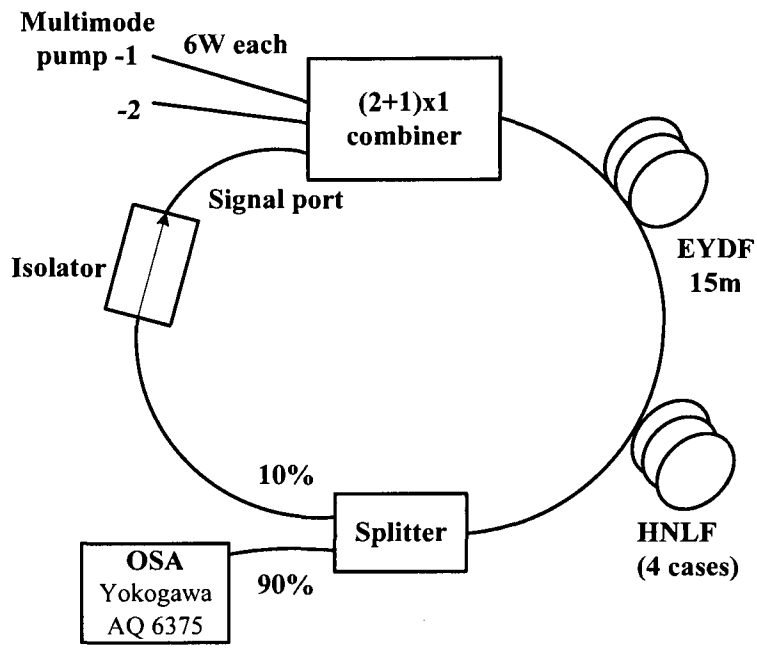

Figure 3.10: Illustration of continuum generation with 90(out):10(in) splitting ratio. The HNLF in the ring is Unit-2(Section 3.2.1), Unit-2+Unit-1(Section 3.2.2), Unit-1+Unit-2(Section 3.2.3) or Unit-1(Section 3.2.4).

For lower loss at high pump power, we cut the two SC/PC connectors of each spool of HNLF and connect it with other components through SMF pigtails by splicing. Splicing loss between two SMF pigtails is almost zero.

3.4.1 Optical Spectrum by using Unit-2 HNLF (~2km) in the Ring

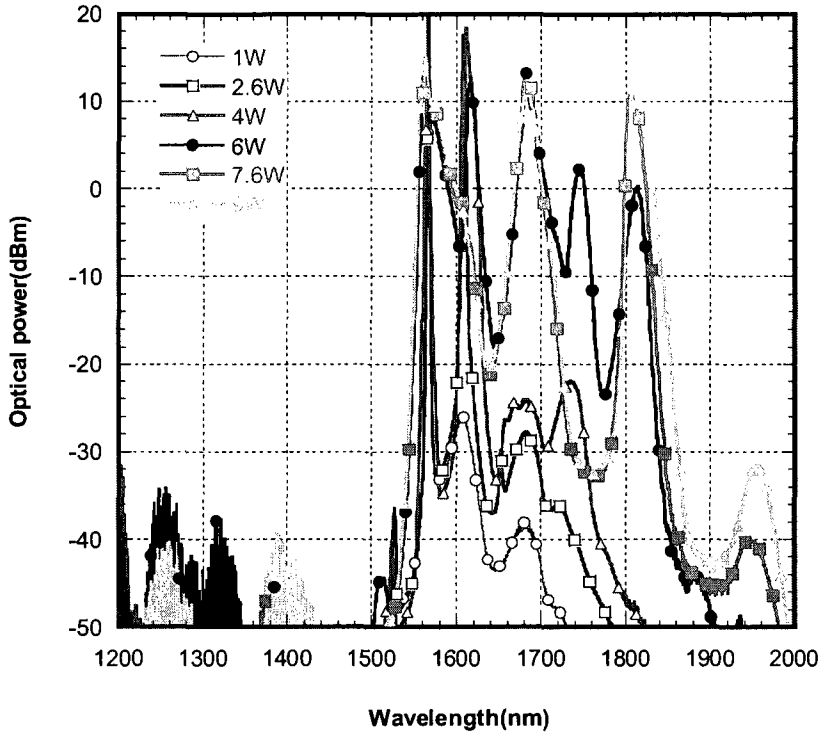

Figure 3.11: Measured optical spectrum versus pump power using only Unit-2 HNLF in the ring.

The Unit-2 fiber is firstly used in the ring laser. Fig. 3.11 shows evolution of the measured optical spectrum versus wavelength with a parameter of 975-nm pump power, where the pump power of 1, 2.6, 4, 6, 7.6 and 9 W is considered. When the pump power is 1 W, it is seen that an optical peak occurs at ~1567 nm and the other peak at ~1608nm appears with the increase of pump power to 2.6W. As explained before, this double-peak is formed by ASE in the EYDF and the ring structure. With further increase of pump power to 7.6 and 9 W, there are many optical peaks coming up in the optical spectrum. The peak at ~1682 nm is the first-order Raman Stokes wave induced by the light beam at ~1567 nm. The peak at ~1744 nm is due to the first-order Stokes wave induced by the light at ~1608 nm. The peak at ~1806 nm is induced by SRS of the light at ~1682 nm.

The small peak at ~1953 nm is due to SRS by the light at ~1806 nm. This fiber (Unit-2) has high negative dispersion parameter (D<0) and this suggests that the MI and FWM effects hardly occur since the linear and nonlinear phase mismatching cannot cancel each other. In other words, SRS, SPM and XPM effects in the Unit-2 fiber occur, and MI and FWM effects hardly occur. It is obviously shown that the optical spectrum is not broadband and flat if only SRS, SPM and XPM occur in the CW based SC generation. By comparison of the pump power at 7.6 and 9 W, it is found that the optical spectrum hardly changes by the increase of the pump power. This further shows that SPM and XPM effects have negligible impact on broadness and flatness of the optical spectrum in CW based SC generation, but SRS effect increases the optical peak at ~1953 nm when the pump power is increased from 7.6 to 9 W.

3.4.2 Optical Spectrum by using Unit-2+Unit-1 HNLF (~3km) in the Ring

Secondly, the Unit-1 fiber is inserted after the Unit-2 fiber in the ring structure, i.e. Unit-2+Unit-1. Fig. 3.12 shows the measured optical spectrum. It is seen that the optical spectrum becomes flatter when the pump power is increased to 6, 7.6 and 9 W. Note that the Unit-1 fiber has anomalous dispersion and thus the MI and FWM effects can occur. It was found that frequency shift by MI effect is in the range of 1-10 THz for pump power of 1-100 W [25]. Therefore, it is believed that the peak at ~1380 nm, which is ~25 THz away from the light at ~1560 nm, is due to FWM between the lights at ~1560 nm and ~1813 nm in the Unit-1 fiber. The broadness around ~1380 nm is due to many FWM effects because there are many FWM interactions between all high peaks. Consequently, the more flatness and broadness of the optical spectrum is due to FWM

that occur in the Unit-1 fiber. This is also because the optical spectrum cannot be extended to ~1380 nm by anti-Stokes wave and MI effect.

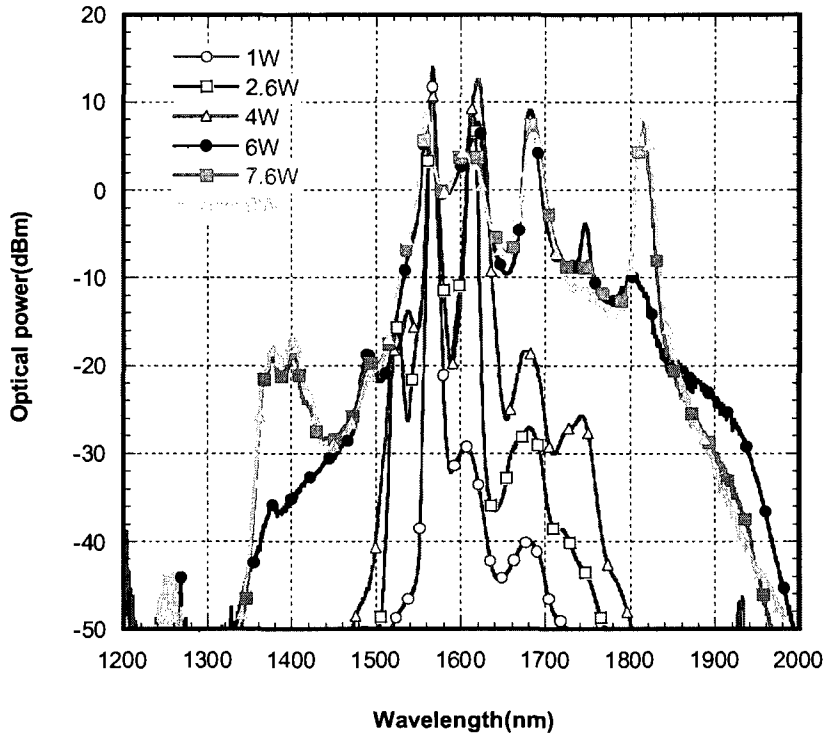

Figure 3.12: Measured optical spectrum versus pump power using Unit-2 and Unit-1 HNLF in the ring.

3.4.3 Optical Spectrum by using Unit-1+Unit-2 HNLF (~3km) in the Ring

Now the order of Unit-1 and Unit-2 fibers in the ring structure is changed, i.e. Unit-1+Unit-2. The measured optical spectrum is shown in Fig. 3.13. It is seen that the optical spectrum is further broader and flatter for high pump power of more than 4 W. For this case, the MI and FWM effects can occur in the Unit-1 fiber in addition to SRS effect. In other words, with the high pump power in the Unit-1 fiber, MI, FWM and SRS effects simultaneously occur and then the generated optical spectrum is further amplified

by SRS effect in the Unit-2 fiber. This is the reason that the optical spectrum in Fig. 3.13 is broader and flatter than in Fig. 3.12.

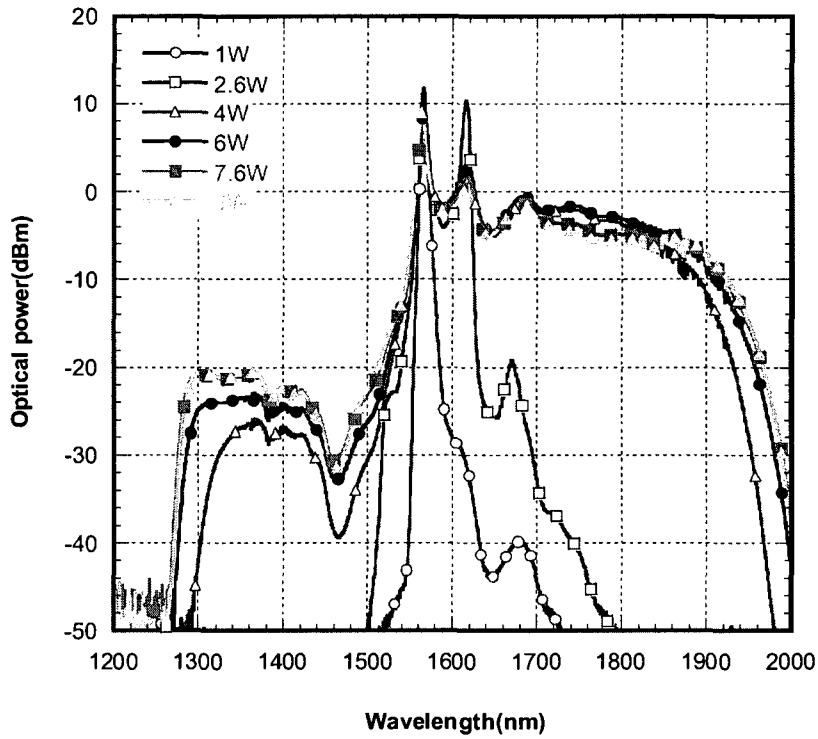

Figure 3.13: Measured optical spectrum versus pump power using Unit-1 and Unit-2 HNLF in the ring.

3.4.4 Optical Spectrum by using Unit-1 (~1km) only in the Ring

Finally only the Unit-1 fiber is inserted in the ring structure. It is observed that with the pump power increased to 7.6 and 9 W, the optical spectrum is further broadened and flattened as shown in Fig. 3.14. A broadband optical SC from 1300nm to 2000nm is obtained with output power of 1.3W (average spectral density is ~-5dBm). It is considered the broadest and highest-power SC generation using multimode 975nm pump lasers. Note that compared to the fiber ring in Section 3.1, output optical power increases from 933mW to ~1.3W because of better connection through splicing than using connectors under high power. Moreover, comparison of optical spectrum in Fig. 3.13 and

in Fig. 3.14 shows that SRS in the additional Unit-2 fiber transfers optical power from short wavelengths to longer wavelengths. This results in the less flatness and broadness of the spectrum in Fig. 3.13.

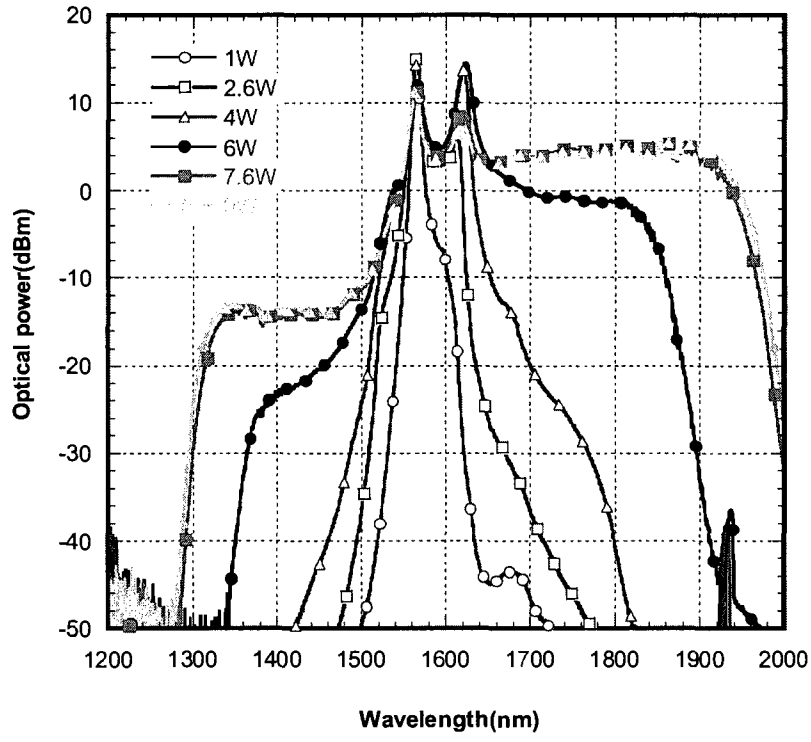

Figure 3.14: Measured optical spectrum versus pump power using only Unit-1 HNLF in the ring.

3.4.5 Comparison of the four Continuums and Output Powers

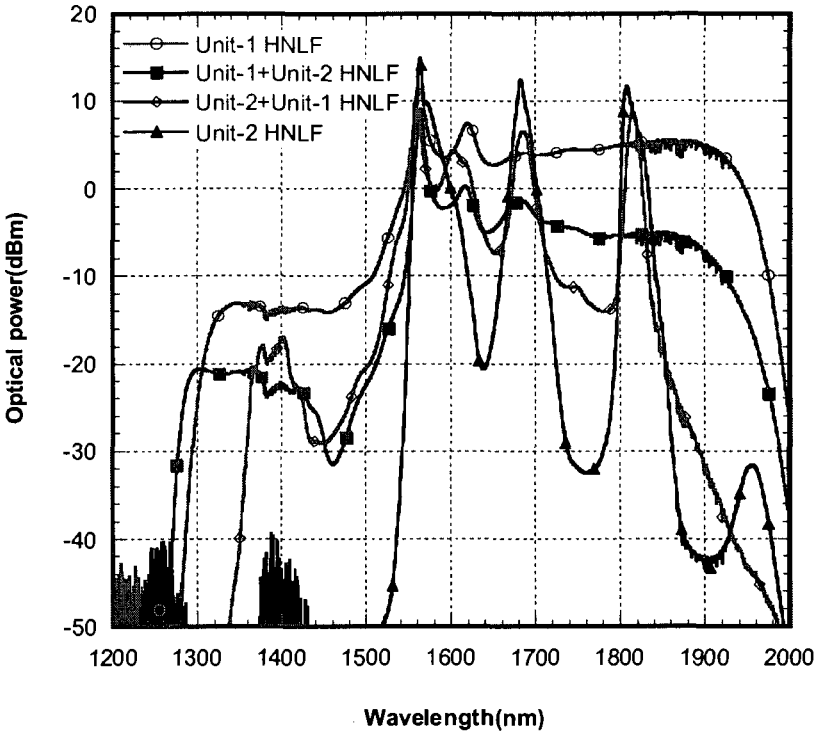

Figure 3.15: Comparison of the generated four optical spectrums at 9W pump.

Fig. 3.15 shows the comparison of the above four spectrums at 9W pump power. The optical spectrums are quite different in both broadness and flatness. Obviously, spectral broadness and flatness increase with the inserting order of Unit-2, Unit-2+Unit-1, Unit-1+Unit-2 and Unit-1 HNLF in the ring. Output optical power as a function of 975-nm pump power for each spectrum is also given in Fig. 3.16. Higher power is detected when only one spool of HNLF is placed in the ring. By using two units of fibers in the ring, output power of both continuums show some kind of saturation at high pump level. Although output optical power is as high as 990mW at 9W pump with Unit-2 HNLF in the ring, the spectrum consists only of four high peaks in the anomalous dispersion region. Despite the different fiber lengths, SRS effect in Unit-1 and Unit-2 is very

similar, to some extent. In other words, the major difference in physical effects is due to the MI and FWM effects in the Unit-1 and Unit-2 fiber since it was found above that SPM and XPM effects are not important in CW based SC generation. Since the MI effect induces a limited broadening, it is believed that the improvement of broadness and flatness in optical spectrum in Fig. 3.14 is mainly contributed by the FWM effect. The optical spectrum from Fig. 3.11 to Fig. 3.14 proves that FWM effect plays a critical role in the CW based SC generation. In addition, it was found that FWM is the key effect for broadening and flattening in ultra-short pulse pumped SC generation [18]. Therefore, convergence in broadening and flattening of SC generation using CW and ultra-short pulse lasers is obtained here.

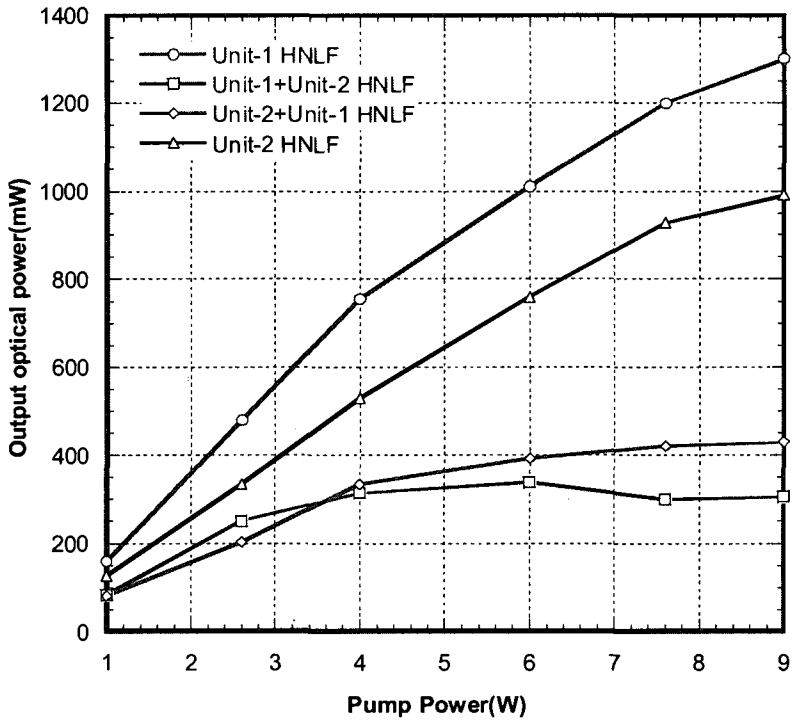

Figure 3.16: Output optical power as a function of pump power at 975nm in the four continuums.

3.5 Advantages of the Ring Structure

Spectrums generated in the above ring structures are very smooth and stable at all pump levels, with all splitting ratios and in all HNLF combinations no matter broadband continuum is formed or not. This shows reasonable and practical of our ring-structure setup.

Moreover, a 1.3 W broadband CW fiber laser source has been demonstrated with ~ 700 nm bandwidth, from 1300nm to 2000nm using low-cost multimode 975-nm pump lasers instead of very expensive fiber Raman lasers and single-mode 1480nm pump lasers. This is considered the broadest CW optical SC generation using multimode 975-nm pump lasers. Except SRS, the nonlinear effect of FWM is found to overwhelm SPM and XPM in the spectral broadening under CW pumping. Compared to previous works [12], it is much more evident that FWM effect plays a significant role in the broadness and flatness of the generated SC.

CHAPTER 4 SUPERCONTINUUM GENERATION USING SINGLE-LINE STRUCTURE

Although the spectrum of the above fiber ring laser extends to the wavelength of 2000nm, narrow bandwidth (40nm) of the splitter in the ring is believed to limit broader SC extension in certain degree. Based on the same components, two other optical fiber lasers using the single-line structure are given in Fig. 2.2. In this chapter, we will evaluate SC performance in this structure and comparisons will also be made between this and the ring-based structure. OSA of Yokogawa AQ6375 with measurable wavelength range of 1200nm to 2000nm is used and 1-nm resolution is taken to record the SC spectrum.

4.1 Supercontinuum Generated by EYDF Ring using Single-line Structure

As shown in Fig. 2.2(a), the splitting ratio used in the ring is 90:10, where 90% light is taken as output and 10% light is fed back to form the EYDF ring. Before light propagating in the HNLF, the spectrum of the EYDF ring is shown in Fig. 4.1. It consists of a narrow peak at ~1567nm and another small broad peak at ~1608nm.

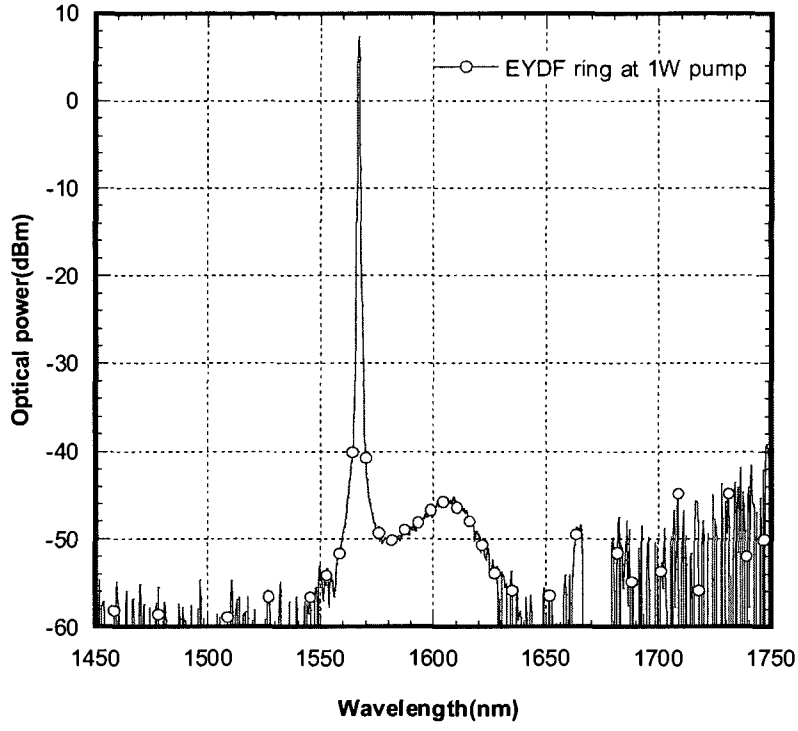

Figure 4.1: Output spectrum of the EYDF ring at 1W pump (OSA Res. =0.05nm).

Then the step in the Section 3.4 is followed. The Unit-1, Unit-2 HNLF and their different combinations are inserted after the EYDF ring in Fig. 2.1(a). The continuous waves as a function of pump power are given in Fig. 4.2.

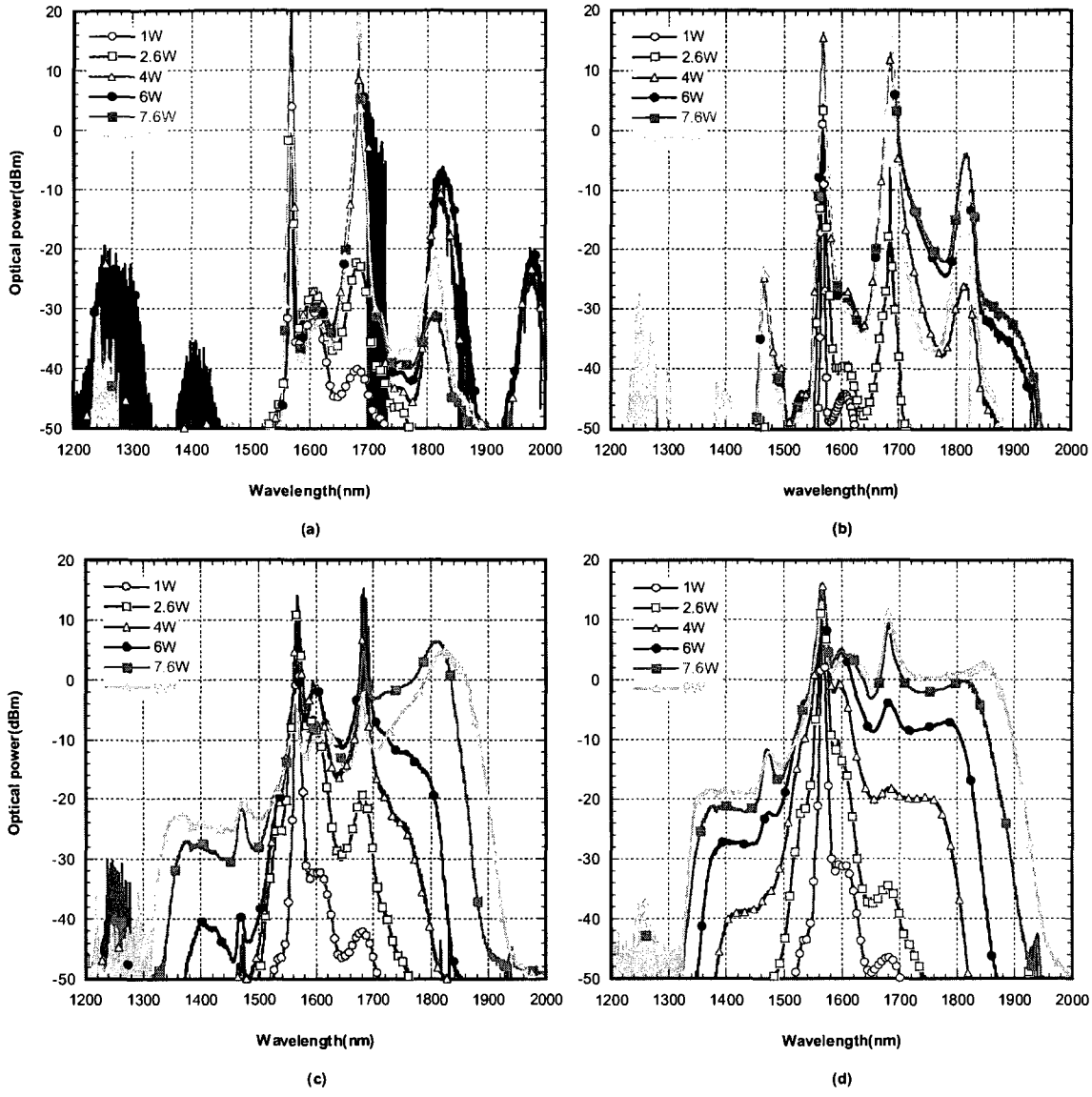

Figure 4.2: SC spectrum versus 975nm pump power driven by EYDF ring laser with (a) Unit-2, (b) Unit-2+Unit-1, (c) Unit-1+Unit-2, and (d) Unit-1 HNLF.

Evolution of the continuum using only Unit-2 HNLF is shown in Fig. 4.2(a). Two peaks at ~1567 nm and ~1608 nm, originally from EYDF ring, can still be observed in the spectrum. Without MI and FWM, strong SRS effect only leads to cascaded Raman Stokes lines in the spectrum, which has been already proved in Fig. 3.11. For example at 6W pump, the peak at ~1682 nm is the first-order Stokes wave of the ~1567 nm peak. It again induces the Stokes line at ~1814nm through SRS. The peak at ~1980nm is the first-

order Stokes line of the ~1814 nm light beam. At 9W pump, the output optical power is also very high that is ~917mW. Fig. 4.3 depicts SC spectrums in the two aforementioned structures at 9W pump by comparing Fig. 4.2(a) and Fig. 3.11. That peaks are much wider in the ring structure indicates that the fiber ring laser experience more nonlinear effects and amplification. It is clear that in Fig. 3.11 the 10% light is continually amplified in the ring until saturation, which lengthens actual interaction length for nonlinear effects at the same pump level.

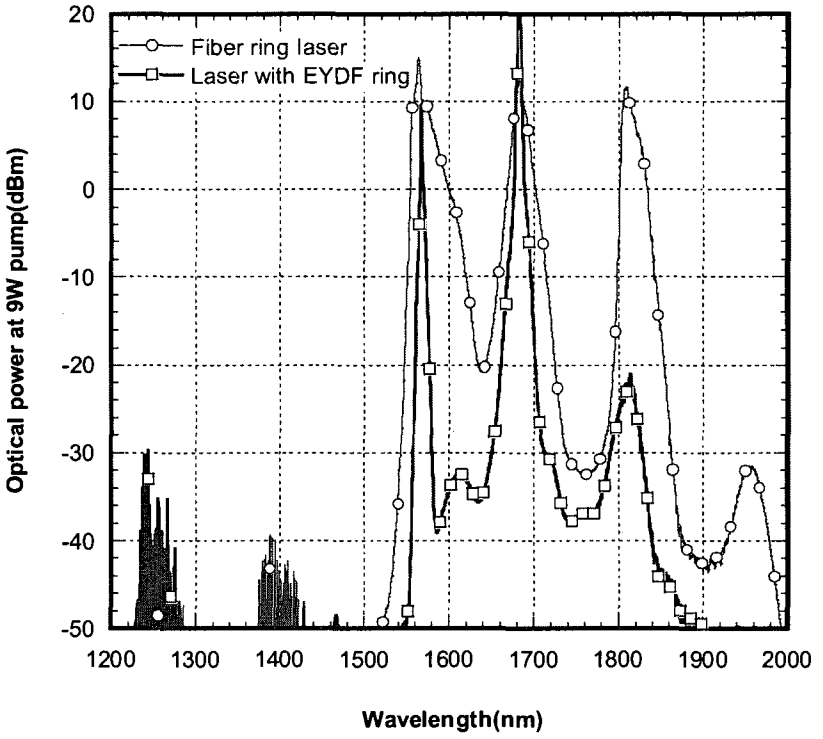

Figure 4.3: SC spectrums in the two designs at 9W pump using the Unit-2 HNLF only.

Spectrum becomes wider from Fig. 4.2 (a) to (d), which proves our explanations again that FWM plays a key role in the CW pumped SC generation. The generated SC in Fig. 4.2(d) is ~570nm wide, which ranges in wavelength from 1350nm-1920nm and optical power is ~1.11W. Three high peaks are observed in the final SC. The 1567nm peak is broadened by SPM and the 1608nm peak experiences gain with increased pump.

The third peak is Raman first-order line at ~1680nm that is maintained in the spectrum with increased pump to 9W. Another small peak at ~1475nm is thought to be generated through FWM by mixing peaks at 1567nm and 1680nm. The spectrum also shows asymmetry by SRS effect.

4.2 Supercontinuum Generation by Backward ASE using Single-line Structure

As illustrated in Fig. 2.2(b), we get rid of the splitter and ring structure and directly take backward ASE light from EYDF to pump the HNLF. A high power optical isolator is inserted before the HNLF to ensure one-direction propagation. One end of the EYDF is angle-cleaved to avoid face reflection. Fig. 4.4(a) shows the broadband ASE spectrum at 1W pump. Three peaks emerge at 1536.0nm, 1544.2nm and 1563.5nm separately. Part of the spectrum is located in the anomalous dispersion region and covers the zero dispersion wavelength of the Unit-1 HNLF, which is required for FWM effect as well as amplification. At the maximum 9W pump, ASE power reaches 2.8W as shown in Fig. 4.4(b).

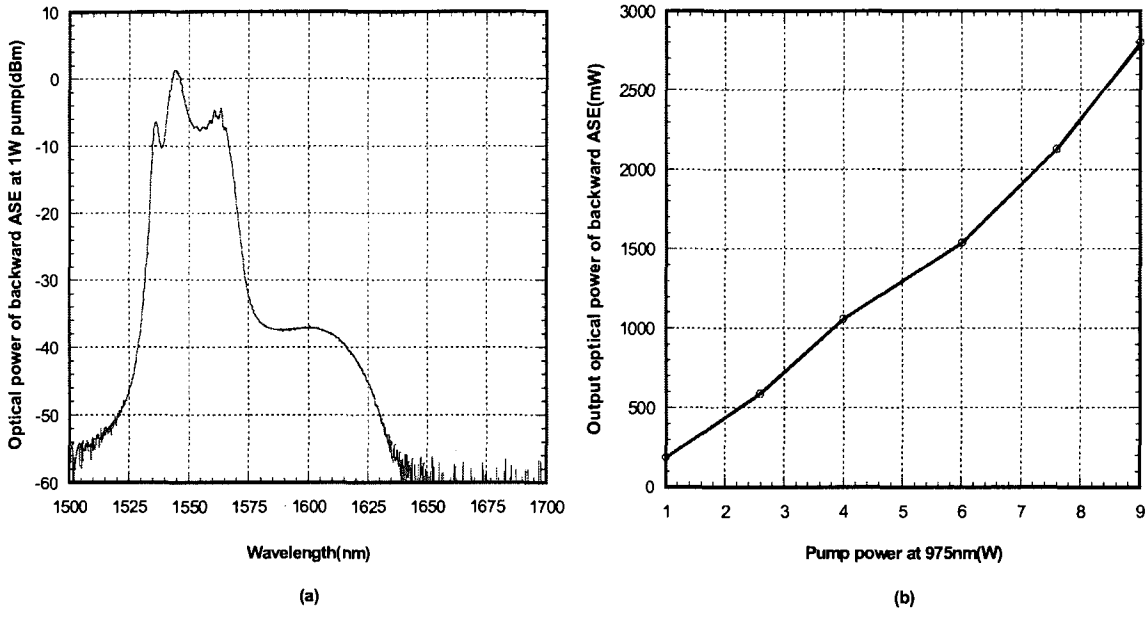

Figure 4.4: Spectrum of the backward ASE of EYDF (OSA Res. =0.05nm) and the ASE power versus 975 pump power.

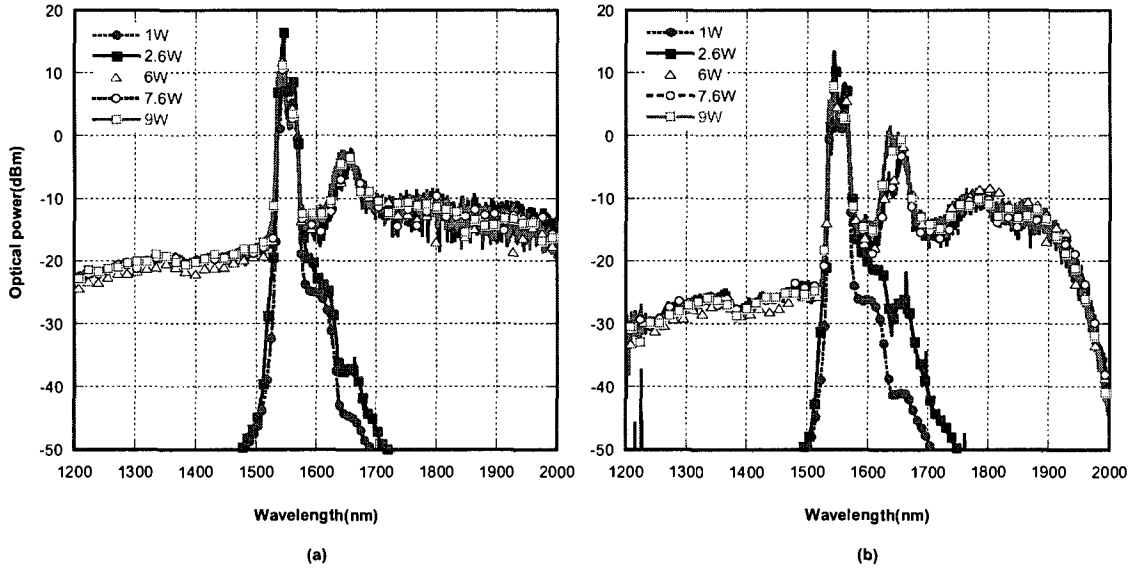

Figure 4.5: Output optical spectrums versus wavelength as a function of pump power using (a) Unit-1 HNLF and (b) Unit-1+Unit-2 HNLF in the backward ASE pumped single-line structure.

Figure 4.5(a) presents the evolution of optical spectrum from the optical supercontinuum generator with only Unit-1 HNLF using pump power of 1, 2.6, 6, 7.6 and 9 W, respectively. At pump power of 1 W, the narrow optical spectrum with three peaks

around 1550 nm is generated. This is due to the backward ASE from the EYDF. With the increase of pump power, the gain peak at 1636.8nm comes up and is due to the first-order Stokes wave by SRS. Also the optical spectrum extends towards short and long wavelength regions. A broadband optical supercontinuum is formed at pump power of 6W. It is seen that the optical supercontinnum extends from 1200 nm to more than 2000 nm with the power level of ~-20 dBm/nm. The total output power is ~257mW (24 dBm). It is seen that there is a little fluctuation of optical power, particularly in the long wavelength range. This may be because our fiber splice is not perfect. Thus many micro-cavities exist between splices and two ends. Consequently fluctuation may occur for high optical powers.

Supercontinuum from 1200nm to almost 2000nm is also observed in Fig. 4.5(b) with Unit-1 and Unit-2 HNLF. Compared to Fig. 4.5(a), the peak at 1636.8nm is higher and it also generates second-order Raman Stokes peak at ~1779.6nm due to strong Raman effect in the Unit-2 HNLF. The formed SC is not very flat from 1600nm to 2000nm and has lower spectral density from 1200nm to 1500nm. Optical power is ~113mW at 9W pump.

Note once the optical supercontinuum is formed, the optical spectrum also hardly changes with further increase of pump power. For example at pump power of 9 W, the optical spectrum is almost the same as the one at the pump power of 7.6 W. The main difference is that the power fluctuation is slightly suppressed at the pump power of 9 W. By optimizing the HNLF length it could be expected that the optical spectrum can be further flattened.

4.3 Evaluation of the Generated Supercontinuums in the Ring and Single-line Structures

Broadband laser sources to wavelength of 2000nm are successfully generated in our three designs with Unit-1 HNLF and Unit-1+Unit-2 HNLF under the co-effects of SPM, XPM, SRS, MI and FWM. Output optical power varies from Watt-level to milli-Watt that is dependent on the designs. The continuum is found to have wider bandwidth, flatter spectrum and higher optical power if only the Unit-1 HNLF is taken, which indicates the importance of SRS interplay with other nonlinear effects together, i.e. FWM and MI, for the contribution of high quality spectrum.

Fig. 4.6 compares the three best generated continuums at 9W pump in Fig. 3.13, 4.2(d) and 4.5(a) using the Unit-1 HNLF only. Formed SC is smoother and more powerful in the first two designs. The fiber ring laser has broader and flatter spectrum than the SC driven by the EYDF ring. In the latter case, the HNLF is not included in the ring. As a result, the effective interaction length for nonlinear effects is relatively short and energy at the ~1680nm Raman peak has not been completely transferred to other parts. The fiber ring laser also shows higher optical power due to re-amplification in the ring. But compared to the ASE pumped SC, the bandwidth of the fiber ring laser is limited by the splitter in the ring. As mentioned before, the splitter used is not broadband (1550±40nm), and propagating light outside this operation window will be highly attenuated. The fall in power at 1900nm-2000nm is caused by the high loss at longer wavelengths and the band limit of the splitter as well.

The three continuums are all low-cost optical supercontinuum sources using low-cost multimode 975-nm pump lasers, an Er/Yb co-doped fiber and the Unit-1 HNLF.

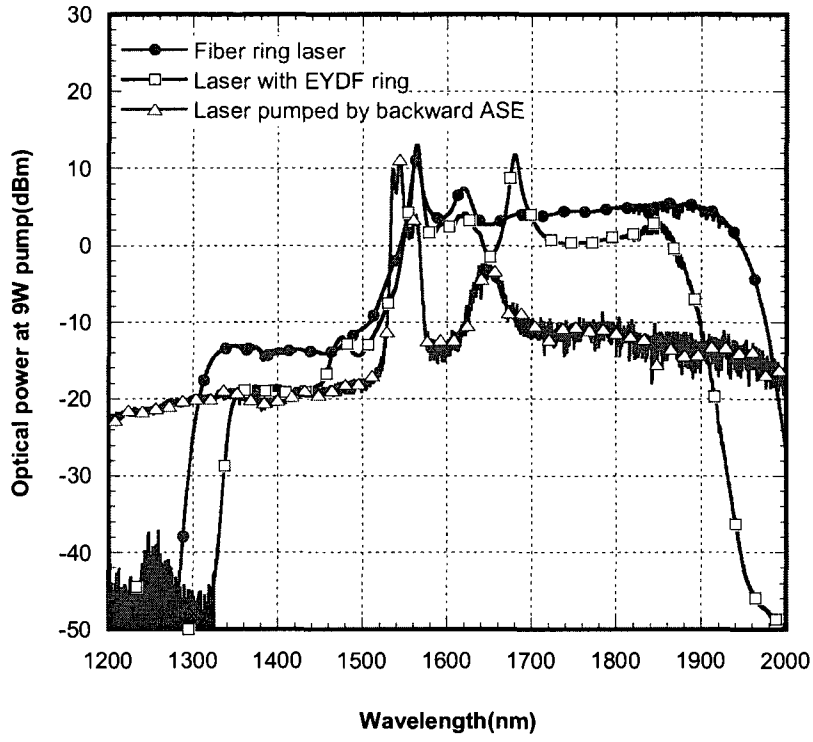

Figure 4.6: Comparison of the three broadband fiber lasers in our experiment using Unit-1 HNLF at 9W pump.

CHAPTER 5 CONCLUSIONS

5.1 Summary

This thesis has been concerned with the design of a low-cost broadband laser source for many applications such as OCT, optical imaging, DWDM, etc. With high power pump sources, nonlinear effects in the fiber lead to frequency shifts by SPM, XPM and SRS, and generate new frequencies through MI and FWM when phase-matching condition is satisfied.

Our setup is low cost and mainly consists of two multimode 975-nm pump lasers, an EYDF, and two units of HNLFs. Three broadband SCs extending to wavelength of 2000nm are successfully generated in different structures: one in the ring structure and the other two in the single-line structure. Firstly, in the ring structure, the optimum splitting ratio on the SC performance is obtained after comparison. The best fiber ring laser is generated with the 90:10 splitter, where 90% power is taken as output and the rest 10% is fed back into the ring. And the generated SC with Unit-1 HNLF in the ring covers an optical spectrum from 1300nm to 2000nm with output power of 1.3W. Except the double-peak from the ring structure, the spectrum is very flat and smooth in the separated two parts. The average spectral density is ~-5dBm. At the same time, roles of different nonlinear effects as well as the importance of FWM in the spectral broadening under CW pumping regime are investigated and demonstrated with combinations of two units of HNLFs in the ring. This demonstration is more evident than previous works.

Secondly, in the single-line structure, a 1.11-W broadband SC from 1350nm to 1920nm in wavelength is formed pumping with EYDF ring. Nonlinear fiber is placed

outside the ring, which decreases the actually interaction length and causes the narrower bandwidth.

Thirdly, a broader SC from 1200nm to more than 2000nm is generated with the backward ASE power from EYDF. To our knowledge, they are the broadest optical SCs with high output power, generated using multi-mode 975-nm pump lasers. By optimizing the HNLF length and using a broadband splitter it is expected that the optical spectrum can be further broadened and flattened.

Above all, our research has explored the new potentiality in the broadband SC generation using low-cost 975nm multimode pumping.

5.2 Future Works

Future researches on the high quality SC will be aimed at high power, broader spectrum (especially in shorter wavelengths) and flatness.

First, the splitter bandwidth is found to limit the SC broadening after comparing the broader SC driven by the backward ASE in Fig. 4.5(a) with the fiber ring laser in Fig. 3.13. Instead, free space splitter could be used in the ring structure for better broadening in the future.

Then, the length of the Er/Yb co-doped fiber amplifier is 15m and not optimized. Because it is very hard to re-splice the star shape fiber together once cut. Better conversion efficiency (ASE power) might be obtained with optimized length.

Third, locations between the ASE peak and the zero dispersion wavelength λ_0 of the HNLF are very important for the FWM effect. By controlling them to improve the

FWM efficiency, center peaks might be able to disappear and transfer energy to other parts, which develop the flatness and increase the total spectral level.

Besides, using double-pump wavelengths and dispersion flatten/decreasing fiber will also be benefit for broadband continuum generation.

REFERENCES

[1] K. Hansen and R. Kristiansen, "Supercontinuum Generation in Photonic Crystal Fibers," Application note on Crystal Fiber A/S website: http://www.crystal-fibre.com/support/Supercontinuum%20-%20General.pdf

[2] S. Smirnov, J. Ania-Castanon, T. Ellingham, S. Kobtsev, S. Kukarin, and S. Turitsyn, "Optical spectral broadening and supercontinuum generation in telecom applications", Optical Fiber Technology, Vol. 12, pp. 122-147, 2006.

[3] T. Kuri, T. Nakasyotani, H. Toda and K. Kitayama, "Characterizations of supercontinuum light source for WDM millimeter-wave-band radio-on-fiber systems," Photonics Tech. Lett, Vol. 17, pp. 1274-1276, 2005.

[4] J. Dudley and S. Coen, "Cohence properties of supercontinuum spectra generated in photonic crystal and tapered optical fibers," Optics Letters, Vol. 27, NO. 13, pp. 1180-1182, 2002.

[5] K. Kim, B. Washburn, G. Wilpers, C. Oates, L. Hollberg, N. Newbury, S. Diddams, J. Nicholson, and M. Yan, "Stabilized frequency comb with a self-referenced femtosecond Cr:forsterite laser", Optics Letters, Vol. 30, Issue 8, pp. 932-934, 2005.

[6] R. Alfano and S. Shapiro, "Emission in the Region 4000 to 7000 Å via four-photon coupling in glass," Phys. Rev. Lett., Vol. 24, pp. 584-586, 1970.

[7] J. Nicholson, A. Abeeluck, C. Headley, M. Yan and C. Jørgensen, "Pulsed and continuous-wave supercontinuum generation in highly nonlinear, dispersion-shifted fibers," Applied Physics B, Vol. 77, pp. 211-218, 2003.

[8] T. Hori, J. Takayanagi, N. Nishizawa, and T. Goto, "Flatly broadened, wideband and low noise supercontinuum generation in highly nonlinear hybrid fiber," Optics Express, Vol. 12, pp. 317-324, 2004.

[9] A. Boucon, D. Alasia, J. Beugnot, G. Melin, S. Lempereur, A. Fleureau, H. Maillotte, J. Dudley, and T. Sylvestre, "Supercontinuum generation from 1.35 to 1.7 μm by nanosecond pumping near the second zero- dispersion wavelength of a microstructured fiber," IEEE Photonics Technol. Lett., Vol. 20, pp. 842-844, 2008.

[10] K. Mori, and K. Sato, "Supercontinuum lightwave generation employing a mode-locked laser diode with injection locking for a highly coherent optical multicarrier source," IEEE Photonics Technol. Lett., Vol.17, pp. 480-482, 2005.

[11] N. Uehara, Y. Takushima, and K. Yasunaka, US patent 2005/0201432, Sept. 2005.

[12] A. Abeeluck, C. Headley and C. Jørgensen, "High-power supercontinuum generation in highly nonlinear, dispersion-shifted fibers by use of a continuous wave Raman fiber laser," Optics Lett., Vol. 29, pp. 2163-2165, 2004.

[13] M. Feng, Y. Li, J. Li, J. Li, L. Ding, and K. Lu, "High-power supercontinuum generation in a nested linear cavity involving a CW Raman fiber laser," IEEE Photonics Technol. Lett., Vol. 17, pp. 1172–1174, 2005.

[14] J. Lee and K. Kikuchi, "Experimental performance comparison for various continuous-wave supercontinuum schemes: ring cavity and single pass structures," Optics Express, Vol. 13, pp. 4848-4853, 2005.

[15] J. Lee, Y. Takushima, and K. Kikuchi, "Continuous wave supercontinuum laser based on an erbium-doped fiber ring cavity incorporating a highly nonlinear optical fiber," Optics Lett., Vol. 30, pp. 2599-2601, 2005.

[16] J. Lee, Y. Han, and S. Lee, "Experimental study on seed light source coherence dependence of continuous-wave supercontinuum performance," Optics Express, Vol. 14, pp. 3443-3452, 2006.

[17] J. Lee, K. Katoh, and K. Kikuchi, "Experimental investigation of continuous-wave supercontinuum ring laser composed of clad-pumped Er/Yb codoped fiber and highly-nonlinear optical fiber," Optics Communications, Vol. 266, pp. 681-685, 2006.

[18] P. Champert, V. Coudere, P. Leproux, S. Fevrier, V. Tombelaine, L. Labonte, P. Roy, C. Froehly and P. Nerin, "White-light supercontinuum generation in normally dispersive optical fiber using original multi-wavelength pumping system," Optics Express, Vol. 12, pp. 4366-4371, 2004.

[19] G. Sefler, W. Mack, G. Valley, and T. Rose, "Secondary energy transfer and non-participatory Yb^{3+} ions in $Er^{3+}-Yb^{3+}$ high-power amplifier fibers," J. Opt. Soc. Am. B, Vol. 21, NO. 10, pp. 1740-1747, 2004.

[20] M. Achtenhagen, R. Beeson, F. Pan, B. Nyman, and A. Hardy, "Gain and noise in ytterbium-sensitized erbium-doped fiber amplifiers: measurements and simulations," Journal of Lightwave Technology, Vol. 19, NO. 10, pp. 1521-1526, 2001.

[21] D. Nguyen, A. Chavez-Pirson, S. Jiang, and N. Peyghambarian, "A novel approach of modeling cladding-pumped highly Er-Yb co-doped fiber amplifiers," IEEE Journal of Quantum Electronics, Vol. 43, NO. 11, pp. 1018-1027, 2007.

[22] E. Yahel and A. Hardy, "Modeling high-power $Er^{3+}-Yb^{3+}$ codoped fiber lasers," Journal of Lightwave Technology, Vol. 21, NO. 9, pp. 2044-2051, 2003.

[23] K. Aiso, Y. Tashiro, T. Suzuki, and T. Yagi, "Development of Er/Yb Co-doped Fiber for High-Power Optical Amplifiers," Furukawa Review, NO. 20, 2001. http://www.furukawa.co.jp/review/fr020/fr20_08.pdf

[24] http://www.nufern.com/specsheets/eydf_7130.pdf, data sheet from Nufern

[25] G. Agrawal, "Nonlinear Fiber Optics," 3rd Edition, Academic Press, San Diego, CA, 2001.

[26] M. Hirano, "Highly nonlinear fibers and their applications," Optical Communications R&D Laboratories, Sumitomo Electric Industries, Ltd., NMIJ-BIPM Joint Workshop, 2007.

[27] O. Toshiaki, H. Masaaki, N. Tetsuya, and O. Masashi, "Highly-nonlinear optical fibers and their applications," SEI Technical Review, NO. 62, pp. 34-40, 2006.

[28] M. Onishi, T. Okuno, T. Kashiwada, S. Ishikawa, N. Akasaka, and M. Nishimura, "Highly nonlinear dispersion-shifted fibers and their application to broadband wavelength converter," Invited paper, Optical Fiber Technology, Vol. 4, pp. 204-214, 1998.

[29] A. Abeeluck and C. Headley, "Supercontinuum growth in a highly nonlinear fiber with a low-coherence semiconductor laser diode," Appl. Phys. Lett., Vol. 85, pp. 4863-4865, 2004.

[30] F. Vanholsbeeck, S. Martin-Lopez, M. González-Herráez, and S. Coen, "The role of pump incoherence in continuous-wave supercontinuum generation," Optics Express, Vol. 13, Issue 17, pp. 6615-6625, 2005.

[31] S. Coen, A. Chau, R. Leonhardt, J. Harvey, J. Knight, W. Wadsworth, and P. Russell, "Supercontinuum generation by stimulated Raman scattering and parametric

four-wave mixing in photonic crystal fibers," J. Opt. Soc. Am. B, Vol. 19, NO. 4, pp. 753-764, 2002.

[32] F. Vanholsbeeck, S. Coen, Ph. Emplit, C. Martinelli, and T. Sylvestre, "Cascaded Raman generation in optical fibers: Influence of chromatic dispersion and Rayleigh backscattering," Opt. Lett., Vol. 29, pp. 998-1000, 2004.

[33] P. Champert, V. Couderc and A. Barthélémy, "1.5-2.0μm Multiwatt Continuum Generation in Dispersion-Shifted Fiber by Use of High-Power continuous-Wave Fiber Source," IEEE Photonics Technology Letters, Vol. 16, NO. 11, pp. 2445-2447, 2004.

[34] S. Li, A. Ruffin, and D. Kuksenkov, "Efficient generation of CW supercontinuum in optical fiber pumped by ASE light," Optical Fiber Communication Conference, 2006 and the 2006 National Fiber Optic Engineers Conference, OFC 2006.

[35] G. Agrawal, "Fiber-optic communication systems," 3rd edition, New York: Wiley-Interscience, 2002.

[36] G. Agrawal, "Lightwave technology: components and devices," Hoboken, NJ : John Wiley, 2004.

[37] K. Abeeluck and C. Headley, "Continuous-wave pumping in the anomalous- and normal-dispersion regimes of nonlinear fibers for supercontinuum generation," Optics Letters, Vol. 30, NO. 1, pp. 61-63, 2005.

[38] C. Giles and E. Desurvire, "Modelling Erbium-Doped Fiber Amplifiers", Journal of Lightwave Technology Letters, Vol. 9, No. 2, pp. 271-283, 1991.

[39] E. Serebryannikova and A. Zheltikov, "Supercontinuum generation through cascaded four-wave mixing in photonic-crystal fibers: When picoseconds do it better", Optics Communications, Vol. 274, Issue 2, pp. 433-440, 2007.

[40] Y. Song, "Ultra wideband CW pumped optical supercontinuum source", Dissertation, Master of Applied Science, Concordia University, 2007.

[41] S. Moon and D. Kim, "Ultra-high-speed optical coherence tomography with a stretched pulse supercontinuum source", Opt. Express, Vol. 14, pp. 11575-11584, 2006.

APPENDIX A DATASHEET OF THE PUMP LASER

EM4 — 6W 975nm 2 Pin Multimode Pump Laser

Features

- 0.15 or 0.22NA 105µm core multimode fiber pigtail
- Uncooled
- Laser welded and epoxy free
- Hermetically sealed
- RoHS compliant
- Qualified high reliability build structure

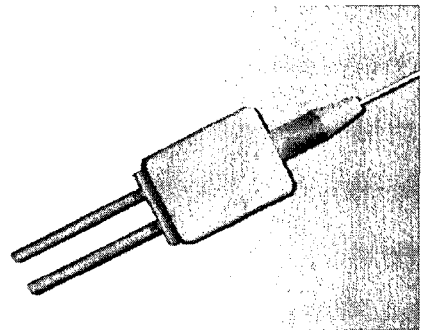

Applications

- Fiber lasers
- Yb laser pumping
- Marking
- Material processing
- Printing

General Description

The EM4 low cost RoHS compliant multimode pump is designed for pumping fiber lasers. It provides 6W of light fiber coupled into a 105µm core multimode fiber with numerical aperture of 0.15 or 0.22. The pump laser chip is built into a 2 pin package. The design and build of the module fulfills the requirements of Telcordia GR-468 and uses EM4 proven manufacturing processes.

Ordering Information

Part Number	λ_C [nm]	Fiber NA
EM304	975	0.15
EM305	975	0.22

Absolute Maximum Ratings

Stresses beyond those listed under "Absolute Maximum Ratings" may cause permanent damage to the device. These are stress ratings only and operation of the device at these or conditions beyond these are not implied. Exposure to absolute maximum ratings for extended periods of time may affect device reliability.

Parameter	Sym	Condition	Min	Max	Unit
Storage Temperature	T_{STG}		-40	85	°C
Operating Case Temperature	T_{OP}		-20	70	°C
Laser Forward Current	I_F			11	A
Laser Reverse Voltage	V_R			2	V
Lead Soldering Time				10	s
Lead Soldering temperature				250	°C
ESD		HBM		500	V

Optical And Electrical Characteristics

T_C=25°C unless otherwise specified, good thermal interface

Parameter	Sym	Condition	Min	Typ.	Max	Unit
Center Wavelength	λ_C	$I=I_{OP}$-1	965	975	985	nm
Operating Current	I_{OP}	$P=P_{OP}$			8	A
Operating Voltage	V_{OP}	$I=I_{OP}$			2.2	V
Output Power	P_{OP}		6			W
Threshold Current	I_{TH}			0.4	0.6	A

EM4 6W 975nm 2 Pin Multimode Pump Laser

Optical And Electrical Characteristics (continued)

T_C=25°C unless otherwise specified.

Parameter	Sym.	Condition	Min	Typ.	Max	Unit
Wavelength Drift vs. T_C	$\delta\lambda/\delta T_C$			0.3		nm/°C
Spectral Width	$\Delta\lambda$	-17dB down from peak		6		nm
Operating Case Temperature	T_C		0		45	°C

Fiber Specification

Parameter	Typ.	Unit
Fiber Type	Step Index	-
Numerical Aperture	0.15 or 0.22	-
Core Diameter	105	µm
Outer Diameter	125	µm
Buffer Diameter	250	µm
Jacket Material	PVDF	-
Jacket Diameter	900	µm
Jacket length from end of boot	85±10	mm
Pigtail Length Min	1	m

Pinning

Pin	Description
1	Laser Anode (+)
2	Laser Cathode (-)

Mechanical Drawing

All units in mm

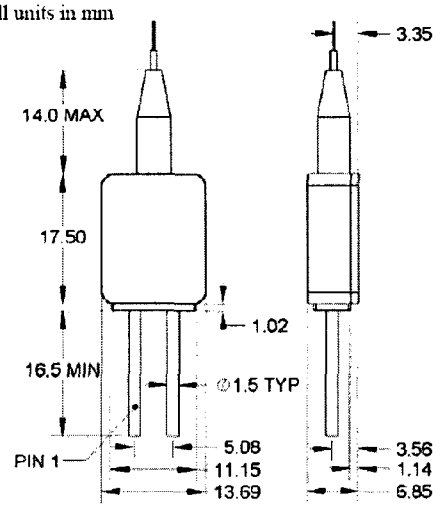

Typical Operating Characteristics

T_C=25°C

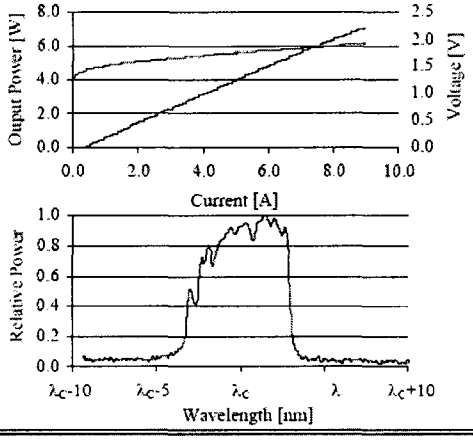

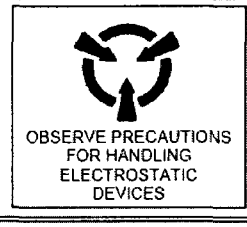

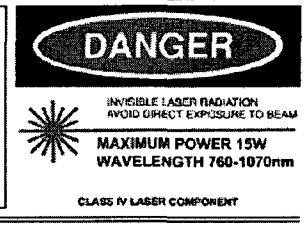

The component complies with all applicable portions of 21 CFR 1040.10, 21 CFR 1010.2 and 21 CFR 1010.3. Since this is a component, it does not comply with all of the requirements contained in 21 CFR 1040.10 and 21 CFR 1040.11 for complete laser products.

For pricing and delivery information, please contact EM4 inc. direct at +1 781 275 75 01, sales@em4inc.com or any of the representatives listed at www.em4inc.com.

APPENDIX B DATASHEET OF THE PUMP COMBINER

PRODUCT SPECIFICATIONS

PART ID: MMC02112A60

Avensys Tech

(2+1) x 1 Multimode Combiner
(105/125 µm NA=0.22 + 8/125 µm NA=0.14/0.46 -> 8/125 µm NA=0.14/0.46)

Pump input port: 105/125µm NA=0.22
Signal port: 8/125µm NA=0.14/0.46
Output port: 8/125µm NA=0.14/0.46

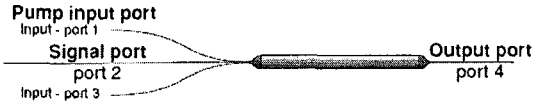

Environmental and Mechanical Specifications	
Power handling	7 W per pump port
Port configuration	(2+1) x 1
Maximum Overall length (L)	65 mm
Diameter (Ø)	3.5 mm
Storage Temperature	-40/ +70 °c
Max Operating temperature	+60°c at the hottest point
Fiber types	
Ports 1 and 3	Multimode fiber 105/125 µm NA=0.22
Port 2	8/125 µm DCF NA=0.14/0.46
Port 4	8/125 µm DCF NA=0.14/0.46
Fiber pigtail length	> 750 mm

➢ Specifications subject to change without notice.

Optical Performance Specifications

PARAMETERS[1]		MIN	MAX		NOTES	PDR
Operating Wavelength – Signal	1530-1560	-	-	nm		
Operating Wavelength – Pumps	900-1000	-	-	nm		
Maximum Insertion Loss – Signal		-	0.35	dB	P2-4	*
Maximum Insertion Loss[2] – Pumps		-	0.5	dB	P1-4 and P3-4	*
Optical Return Loss[2] - Pump		35	-	dB	P1-1 and P3-3	*

[1] Parameters are specified at room temperature
[2] Fully filled conditions

APPENDIX C DATASHEET OF THE EYDF

CLADDING PUMPED FIBERS
Specification Sheet

Erbium-Ytterbium Cladding Pumped Fibers

130 µm

ofs
Leading Optical Innovations

Product Description

The 125 µm single-mode core of this fiber is co-doped with both erbium and ytterbium. It is then surrounded by a silica cladding and covered with a low-index protective coating. The resulting double-clad fiber is used for single-mode fiber lasers and amplifiers operating in the 1540 to 1565 nm range.

The fiber enables fiber lasers and amplifiers with good beam profile characteristics, high wall-plug efficiencies, compact foot prints, superior reliability, and maintenance-free operation. It also accommodates high energies during pulsed operation and at high repetition rates.

Typical Applications

- Construction of multi-watt amplifiers around 1550 nm

Features and Benefits

- Active ion concentrations optimized for efficiency
- High erbium concentration for short devices
- Wide pump wavelength window from 910 to 1060 nm
- Low-splice-loss achieved to conventional single-mode or dispersion-shifted fiber

Related Products & Capabilities

- PM Erbium-Ytterbium Cladding Pumped Fibers
- SM Cladding Pumped Fiber Lasers
- Single-mode PowerMAX Combiners
- Erbium-Ytterbium Gain Modules

Ask us about other options available:

- ☑ **ErYb Gain Modules**
- ☑ **PM Erbium-Ytterbium Fibers**
- ☑ **ClearLite Single-Mode Fibers**
- ☑ **Custom Designs**

To order items on this spec sheet, please contact our facility in:

- ☑ Somerset, New Jersey 1-732-748-7402
- ☑ or by email inquiry to: Info@SpecialtyPhotonics.com

ofs
Leading Optical Innovations
OFS Specialty Photonics Division
55 Darling Drive, Avon, CT 06001
25 Schoolhouse Road, Somerset, NJ 08873
Priorparken 680 DK-2605 Broendby, Denmark
www.SpecialtyPhotonics.com

Fiber Specifications (typical)

Properties	ErYb 130
Core numerical aperture	0.17
Cladding numerical aperture	0.45
Cutoff wavelength	<1540 nm
Mode field diameter @ 1550 nm	7 µm
Ytterbium clad absorption @ 915 nm	>0.5 dB/m
Erbium peak absorption near 1535 nm	40 dB/m
Star cladding diameter	130 µm
Coating outer diameter	250 µm
Mechanical and Testing Data	
Proof test level	100 kpsi
Order by Part Number (also specify fiber length in meters)	**108 728 635**

Cladding Pumped Fiber Design

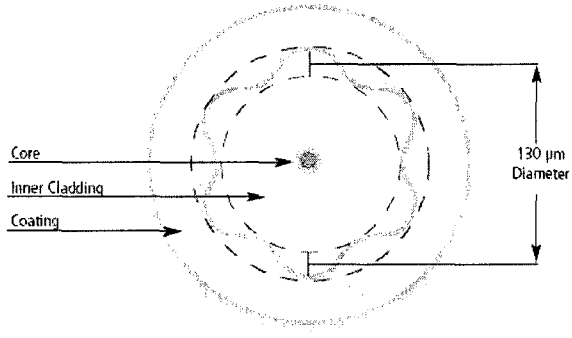

Erbium/Ytterbium Codoped CPF Data Sheet

ofs
A Furukawa Company

Fiber Type: **EY125-SM-S**

Lot No.: **EY623101**

Part Number: **108728635**

Cladding Pumped Fiber Design

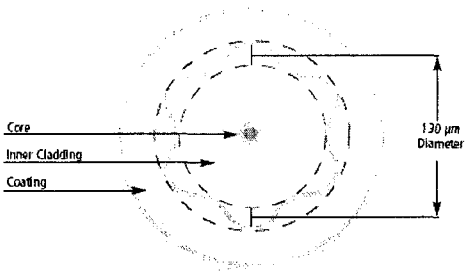

Parameter	Value	Parameter	Value
Er peak absorption (near 1530nm)[1]	48dB/m	MFD @ 1550nm (Peterman II)	6.5 µm
Background loss @ 1150nm	20 dB/km	Cladding numerical aperture	0.45
Est. Cladding absorption @ 920nm	0.9 dB/m	Core Concentricity Error	<.3 µm
Core numerical aperture	0.199	Proof test	>100 kpsi
LP_{11} cutoff wavelength	1320nm	Core diameter	5.8 µm
1. Core absorption 2. Fiber OD +/- 5 µm, 3. Coating OD+/- 15 µm		Fiber outside diameter[2]	130 µm
		Coating outside diameter[3]	260 µm
		Coating Type	PowerClad

APPENDIX D DATASHEET OF THE TWO UNITS OF HNLFS

SM-HNLF TECHNICAL PARAMETERS AND DESCRIPTION

Highly Nonlinear Optical Fibre Unit 1		
Fiber Product Origin		Tokyo, Japan
Manufacturer Name		Sumitomo Electric Industries, Ltd.
Date of manufacture		July 16, 2002
Manufacturer Part Number		DC490AB-4
Manufacturer Serial Number		788-8304-01
Total Fiber Length		1210 meter
Cut-off Wavelength		1550 nm
Total Insertion Loss @ 1310 nm		1.16 dB
Unit Insertion Loss @ 1310 nm		0.95 dB/km
Total Insertion Loss @ 1550 nm		0.654 dB
Unit Insertion Loss @ 1550 nm		0.54 dB/km
At 1550nm	Dispersion	-0.8 ps/nm/km
	Dispersion slope	0.03 $ps/nm^2/km$
	gR/A_{eff}	6.18 $(W-km)^{-1}$
	A_{eff}	$10\mu m^2$
Nonlinear coefficient		12 $(W-km)^{-1}$
PMD		0.1 $ps/\sqrt{km}$
Pigtail (both ends)		0.9 mm Jacked SMF × 1.5 meters length
Connector (both ends)		SC/PC
Adaptor (both ends)		SC
Working Condition		Very Good

SM-HNLF TECHNICAL PARAMETERS AND DESCRIPTION

Highly Nonlinear Optical Fibre Unit 2		
Fiber Product Origin		Tokyo, Japan
Manufacturer Name		Sumitomo Electric Industries, Ltd.
Date of manufacture		July 16, 2002
Manufacturer Part Number		DC1169D-1
Manufacturer Serial Number		788-8302-01
Total Fiber Length		2490 meter
Cut-off Wavelength		1370 nm
Total Insertion Loss @ 1310 nm		4.904 dB
Unit Insertion Loss @ 1310 nm		1.964 dB/km
Total Insertion Loss @ 1550 nm		1.743 dB
Unit Insertion Loss @ 1550 nm		0.7 dB/km
At 1550nm	Dispersion	-12 ps/nm/km
	Dispersion slope	0.01 ps/ nm^2 /km
	gR/A_{eff}	6.0 $(W - km)^{-1}$
	A_{eff}	10 μm^2
Nonlinear coefficient		12 $(W - km)^{-1}$
PMD		0.1 ps/$\sqrt{km}$
Pigtail (both ends)		0.9 mm Jacked SMF × 1.5 meters length
Connector (both ends)		SC/PC
Adaptor (both ends)		SC
Working Condition		Very Good